

# Multi-omics identify LRRC15 as a COVID-19 severity predictor and persistent pro-thrombotic signals in convalescence

Jack S. Gisby<sup>\*1</sup>, Norzawani B. Buang<sup>\*1</sup>, Artemis Papadaki<sup>1</sup>, Candice L. Clarke<sup>1,2</sup>, Talat H. Malik<sup>1</sup>, Nicholas Medjeral-Thomas<sup>1,2</sup>, Damiola Pinheiro<sup>1</sup>, Paige M. Mortimer<sup>1</sup>, Shanice Lewis<sup>1</sup>, Eleanor Sandhu<sup>1,2</sup>, Stephen P. McAdoo<sup>1,2</sup>, Maria F. Predecki<sup>1,2</sup>, Michelle Willicombe<sup>1,2</sup>, Matthew C. Pickering<sup>1</sup>, Marina Botto<sup>1</sup>, David C. Thomas<sup>†1,2</sup>, James E. Peters<sup>†1</sup>

\*equal contributions  
†jointly supervised the work

## Author Affiliations

1) Centre for Inflammatory Disease, Dept of Immunology and Inflammation, Imperial College London.  
2) Renal and Transplant Centre, Hammersmith Hospital, Imperial College Healthcare NHS Trust, London, United Kingdom.

Correspondence to: James E. Peters or David C. Thomas. Email: [j.peters@imperial.ac.uk](mailto:j.peters@imperial.ac.uk) or [david.thomas1@imperial.ac.uk](mailto:david.thomas1@imperial.ac.uk)

## Abstract

Patients with end-stage kidney disease (ESKD) are at high risk of severe COVID-19. Here, we performed longitudinal blood sampling of ESKD haemodialysis patients with COVID-19, collecting samples pre-infection, serially during infection, and after clinical recovery. Using plasma proteomics, and RNA-sequencing and flow cytometry of immune cells, we identified transcriptomic and proteomic signatures of COVID-19 severity, and found distinct temporal molecular profiles in patients with severe disease. Supervised learning revealed that the plasma proteome was a superior indicator of clinical severity than the PBMC transcriptome. We showed that both the levels and trajectory of plasma LRRC15, a proposed co-receptor for SARS-CoV-2, are the strongest predictors of clinical outcome. Strikingly, we observed that two months after the acute infection, patients still display dysregulated gene expression related to vascular, platelet and coagulation pathways, including *PF4* (platelet factor 4), which may explain the prolonged thrombotic risk following COVID-19.

## Introduction

COVID-19, caused by the SARS-CoV-2 virus, is a highly heterogenous disease. In most individuals, it is a mild, self-limiting illness, but some individuals develop severe disease, typically manifesting as respiratory failure with marked systemic inflammation and immunopathology. Multiple studies have described immunological [1,2], transcriptomic [3–7], and proteomic [8–16] correlates of severe disease. The importance of an aberrant host immune response in tissue injury in severe COVID-19 is supported by the efficacy of anti-inflammatory treatments. These include glucocorticoids [17], monoclonal antibodies blocking the interleukin-6 receptor [18,19], and the Janus kinase (JAK) inhibitor baricitinib [20]. A wide range of additional therapies directed at specific elements of the inflammatory response has been developed for immuno-inflammatory diseases and present potential repurposing opportunities for the treatment of severe COVID-19. Understanding the molecular basis for severe COVID-19 is critical for the rational selection of such therapies.

Risk factors for severe COVID-19 include age, male sex, and the presence of comorbidities such as chronic kidney disease (CKD). In CKD, the risk of severe COVID-19 is proportional to the degree of renal impairment [21]. End-stage kidney disease (ESKD) confers particularly high risk, with a population-based study estimating a hazards ratio for death of 3.69 [21] and a European registry study reporting 23.9% 28-day mortality in dialysis patients with COVID-19 [22]. In part, this is because ESKD patients are enriched for other risk factors for severe COVID-19, including cardiometabolic disease. However, even after adjustment for these,

ESKD remains independently associated with the risk of severe COVID-19. In addition, ESKD patients display impaired vaccine responses [23,24], and those on haemodialysis cannot shield effectively during lockdowns as they need to access dialysis facilities regularly.

Here, we investigated the host response to SARS-CoV-2 in ESKD patients on haemodialysis since study of such an at-risk group should enhance the probability of identifying severity signals and might also point to either an exaggerated or even distinct immunological response to the virus. Moreover, ESKD patients receiving haemodialysis present a unique opportunity for serial blood sampling of both outpatients and inpatients with COVID-19, since patients must attend medical facilities for regular dialysis regardless. This enabled us to perform longitudinal analysis and avoid the selection bias that affects studies limited solely to hospitalised patients.

The host response to SARS-CoV-2 is orchestrated by a complex network of cells and mediators, including circulating proteins such as cytokines and soluble receptors. Soluble proteins play key roles in multiple biological processes, including signaling, host defence and repair, and are potential biomarkers and therapeutic targets. We therefore hypothesised that a comprehensive analysis of both circulating proteins and immune cells should yield valuable and complementary insights into the pathobiology of COVID-19. To this end, we used the aptamer-based SomaScan platform that provides the broadest available coverage of the plasma proteome (6,323 proteins), combined with RNA-sequencing and flow cytometry of peripheral blood mononuclear cells (PBMCs). We integrated these data to provide a comprehensive view of the COVID-19 multi-omic landscape, enabling us to link transcriptomic and cellular changes with circulating proteins. Supervised learning identified plasma levels of the LRR15 protein, a recently proposed alternative receptor for SARS-CoV-2, as a key marker of disease severity. Uniquely, by comparing pre-infection samples to samples collected from the same individuals during COVID-19 and after clinical recovery, we revealed persistent upregulation of gene expression signatures related to vascular and clotting pathways several months after infection. These findings elucidate the biological underpinnings of the prolonged pro-thrombotic state associated with COVID-19.

## Results

### Features of patient cohorts

We recruited two cohorts of ESKD patients on haemodialysis presenting with COVID-19 (**Figure 1A**). The Wave 1 cohort consisted of 53 patients recruited during the initial phase of

the COVID-19 pandemic (April-May 2020) (**Supplementary Table 1**). Serial blood sampling was carried out where feasible (**Figure 1B**), given the pressure on hospital services and the effects of national lockdown. We assessed disease severity using a WHO four-level ordinal score, categorising it into mild, moderate, severe, and critical. Of the 53 patients, 25 had a peak illness severity score of severe or critical (hereafter ‘severe/critical’) and 28 mild or moderate (‘mild/moderate’). Nine died. The majority of patients were of non-European ancestry. Further clinical and demographic details are provided in **Supplementary Table 1**. We also contemporaneously recruited 59 non-infected haemodialysis patients to provide a control group, selected to mirror the age, sex and ethnicity distribution of the COVID-19 cases (**Supplementary Figure 1A-C**).

The Wave 2 cohort consisted of 17 ESKD patients with COVID-19 infected during the resurgence of cases in January-March 2021 (**Supplementary Table 2**). All had been recruited as part of the COVID-19 negative control group during Wave 1, thereby providing a pre-infection sample collected 8-9 months earlier. For the Wave 2 cohort, we systematically acquired serial samples for all patients at regular intervals (every 2-3 days over the course of the acute illness) (**Figure 1C**). 9 patients had a peak illness severity of severe/critical (of whom 4 died), and 8 mild/moderate. For 12 of these patients, we acquired convalescent samples approximately two months following infection.

# The effect of COVID-19 on the PBMC transcriptome and plasma proteome in ESKD patients

We performed transcriptomic profiling using RNA-seq of PBMCs. Principal components analysis (PCA) revealed a clear effect of COVID-19 in both Wave 1 (COVID-19 positive and negative patient samples) and Wave 2 (pre-infection and subsequent COVID-19 positive samples from the same individuals) (**Figure 2A**). In the Wave 1 cohort, differential gene expression analysis between COVID-19 positive (n=179 samples from 51 patients) and negative samples (n=55) using linear mixed models (LMM) identified 3,026 significantly up-regulated and 3,329 down-regulated genes (1% false discovery rate, FDR) (**Supplementary File 1A**). For the Wave 2 cohort, where we compared COVID-19 positive samples (n=90 samples from 17 individuals) with pre-infection samples from these same individuals, we identified 2,871 up-regulated and 3,325 down-regulated genes (1% FDR, LMM) (**Supplementary File 1A**). These findings demonstrate widespread transcriptomic changes associated with COVID-19. The effect sizes for the differentially expressed genes between the Wave 1 and 2 cohorts were highly concordant (Pearson’s r 0.80) (**Supplementary Figure 2A**), despite differences in the prevalent SARS-CoV-2 variant and developments in medical management (8 of 17 patients in the Wave 2 cohort received glucocorticoids). To identify the

genes that were consistently differentially expressed across both cohorts, we used robust rank aggregation (RRA) (**Supplementary File 1A, Supplementary Figure 3**).

To gain insight into the biological pathways underlying these changes, we used Gene Set Variation Analysis (GSVA) [25] to compare COVID-19 positive and negative ESKD samples (**Supplementary File 1B**). Enriched pathways included those related to cell cycle (e.g. “Polo-like kinase mediated events”, which are involved in the cellular response to DNA damage) and host defence (e.g. “Complement cascade”, “Fc-gamma receptor-dependent phagocytosis”, and “Parasite infection”) (**Supplementary Figure 4**). This analysis also highlighted leukocyte-endothelial interactions (“Cell surface interactions at the vascular wall”, which included *SELL* and *CEACAM-1*, -3, -6 and -8 genes). Examples of marked changes in gene expression between the pre-infection and first acute infection sample in the Wave 2 cohort included components of “Immunoregulatory interactions between a lymphoid and a non-lymphoid cell” pathway term (e.g. *SIGLEC1*, *SIGLEC9*, *SELL*, all increased) and “Development and heterogeneity of the ILC family” (e.g. *IFNG*, *GATA3*, *RORA*, all decreased) (**Figure 2B**).

We next assessed the circulating proteome, measuring 6,323 proteins using the SomaScan platform (**Supplementary File 1C**). PCA showed clear differences between COVID-19 positive and negative samples (**Figure 2A**). We identified 1,273 differentially abundant proteins between COVID-19 positive and negative samples in Wave 1 (86 samples from 37 COVID-19 positive ESKD patients versus 53 non-infected ESKD patient samples, LMM) (**Supplementary File 1D, Supplementary Figure 5**). In Wave 2, comparison of COVID-19 positive samples (n=102 samples from 17 patients) with pre-infection samples from the same individuals identified 5,265 differentially abundant proteins. The effect sizes were generally concordant between the cohorts (Pearson’s  $r$  0.57) (**Supplementary Figure 2B**). As for our transcriptomic analysis, we used RRA to identify the differentially abundant proteins consistent across both cohorts (**Supplementary File 1D**).

Enrichment analysis revealed upregulation of pathways, including “DDX58 IFIH1 mediated induction of interferon-alpha/beta”, “Wilk *et al.*, 2021 IFN module” [26], “Host-pathogen interaction of human coronaviruses interferon induction” and “SARS-CoV-2 innate immunity evasion and cell-specific immune response”, reflecting host anti-viral responses and providing validation of our analysis (**Figure 2C, Supplementary File 1E**). Highly up-regulated proteins within these pathways included STAT1; DDX58 and ISG15, both crucial to the IFN-mediated antiviral response in COVID-19 [27]; IFITM3, which is up-regulated in lung epithelial cells during early SARS-CoV-2 infection [28]; and the chemokines CXCL11, CXCL1, CXCL6, CXCL5 and CXCL10. Another significantly up-regulated pathway was “Senescence-

associated secretory phenotype”, which included up-regulated ubiquitin-conjugating enzymes (UBE2S, UBE2E1), histones (H2BC21, H2BU1) and STAT3 (**Figure 2D**). Down-regulated pathways included “Integrin cell surface interactions” and “Collagen biosynthesis and modifying enzymes” which contained collagen proteins (e.g. COL11A2, COL13A1, COL15A1) and related enzymes (e.g. P4HB, PCOLCE) (**Figure 2D**).

# Transcriptomic and proteomic changes associated with COVID-19 severity

In both cohorts, the PCA of the PBMC transcriptomics revealed differences according to both severity at time of sampling and overall clinical course (defined by peak severity score) (**Figure 3A**). There was a gradient of severity reflected in the molecular phenotype. We next assessed molecular features associated with severity at time of blood sampling, encoded as an ordinal variable. We identified 3,522 genes that were significantly associated with contemporaneous severity in the Wave 1 cohort and 657 genes in the Wave 2 cohort (LMM, 1% FDR, **Supplementary File 1F, Supplementary Figure 6**). We then applied GSVA to identify pathways and used RRA to combine results from each cohort (**Supplementary File 1G**).

The up-regulated transcriptomic pathways in more severe disease included those involved in oxidative stress (“Glutathione metabolism”, “Detoxification of reactive oxygen species”), “Transcriptional regulation of granulopoiesis”, pathways containing numerous histone-encoding genes (“HDACs deacetylate histones”, “Diseases of programmed cell death”, “RHO GTPases activate PKNs”) and “Complement and coagulation cascades” (**Figure 3B-C, Supplementary File 1G**). Down-regulated pathway terms included “TCRA pathway”, “Pathogenesis of SARS-CoV-2 mediated by nsp9-nsp10 complex”, “TP53 activity”, and “PD1 signaling”, suggesting T cell activation in more severe COVID-19 (**Figure 3B-C, Supplementary File 1G**).

PCA of the proteomic data revealed differences according to clinical severity (**Supplementary Figure 7A**). We found 148 and 1,625 proteins associated with disease severity in the Wave 1 (86 COVID-19 positive samples) and Wave 2 (102 COVID-19 positive samples) datasets, respectively (**Supplementary File 1H, Supplementary Figure 8**). Pathway analysis identified 15 severity-associated pathway terms that reached statistical significance (1% FDR) in both cohorts (**Supplementary Figure 7B, Supplementary File 1I**). Among the most upregulated pathways in more severe disease were “HDACs deacetylate histones”, pathways related to transcriptional regulation (e.g. “mRNA splicing minor pathway”, “Spliceosome”, “RNA polymerase II transcription termination”, “Processing of capped intron-containing pre mRNA”) and “RUNX1 regulates genes involved in megakaryocyte differentiation and platelet function”,

while the most down-regulated pathways included “PD-1 signaling” and “T-cell receptor and costimulatory signaling”. Example proteins from these pathways are shown in **Supplementary Figure 7C**.

# Severe COVID-19 is associated with dynamic multi-omic modular trajectories

We next examined the temporal trajectories of the transcriptome and the proteome during COVID-19 by explicitly modelling molecular profiles with respect to time following symptom onset (**Methods**). To aid biological interpretation, we first applied a dimension reduction strategy using weighted gene correlation network analysis (WGCNA) [29]. WGCNA identified 23 modules of co-expressed genes (which we denote with the prefix ‘t’) (**Supplementary File 1J**), and 12 proteomic modules (denoted with ‘p’) (**Supplementary File 1K**). Longitudinal modelling revealed 8 transcriptomic and 5 proteomic modules with significantly (5% FDR) different temporal patterns in patients with mild/moderate versus severe/critical disease (LMM time x clinical course (TxCC) interaction - **Methods**) (**Supplementary Tables 3-4**). Typically, the modules displayed a flat temporal profile in mild/moderate COVID-19, whereas there was a dynamic profile in severe/critical disease (**Figure 4A**, **Supplementary Figure 9**). Some modules rose with time in severe/critical patients (e.g. tB, tL, p9 and p12), whilst others dropped (e.g. tC, tP, tI, p7). Examples of individual genes from module tB exhibiting this behaviour include *MMP9*, *ORM1*, *LRRN1* (**Figure 4B**).

We identified significant associations between modules, with transcriptomic and proteomic modules clustered into larger positively or negatively correlated groupings (**Figure 4C**). The inter-modular associations appeared to strongly reflect association with COVID-19 severity at time of sampling (**Supplementary Tables 3-4**), implying that this is a strong underlying factor in the -omics data. Consistent with this, integrated analysis of the transcriptomic and proteomic datasets using MEFISTO [30] revealed a single factor that had a significantly different trajectory in severe/critical versus mild/moderate disease ( $p < 0.0001$ , LMM TxCC) (**Supplementary Figure 10**).

We characterised the modules by pathway analysis (**Figure 4A**, **Supplementary Tables 3-4**, **Supplementary File 1L**, **Supplementary File 1M**). We also investigated whether disease trajectory-associated transcriptomic modules might reflect a shift in cell-type proportions, estimated using the CIBERSORTx algorithm (**Methods**) (**Supplementary Figure 11**, **Supplementary File 1N**). The severity-associated modules tB and tJ were both strongly positively associated with myeloid cell proportions, particularly neutrophils, and negatively associated with lymphocyte subsets (**Supplementary Figure 11**). The presence of a

neutrophilic gene signature in the PBMC preparations may indicate the presence of low-density granulocytes. Consistent with this, hub genes in Module tB (including *TECPR2*, *CSF3R*, *STX3*; **Figure 4A**) are associated with granulocytes and autophagy, and pathway analysis of the module genes revealed enrichment for pathways including “Neutrophil degranulation” and “ROS and RNS production in phagocytes” (including genes encoding the key cytosolic components of the phagocyte NADPH oxidase such as *NCF1*, *NCF2* and *NCF4*). Module tB also contains genes encoding calcium-binding proteins (e.g. *S100A6*, *S100A9*, *S100A11*, *S100A12*) that play important roles in regulating inflammatory pathways [31], as well as integrins (e.g. *ITGA1*, *ITGAM*, *ITGB4*, *ITGAX*, *ITGAD*), adhesion molecules (e.g. *CEACAM1*, *CEACAM3*, *CEACAM4*, *ICAM3*), *OSM* (encoding Oncostatin M) and *CSF1* (encoding M-CSF). The tL module, which also displayed a rising trajectory in worse disease, was strongly positively associated with imputed plasma cell proportion (**Supplementary Figure 11**) and many of its members encoded immunoglobulins. The severity-associated proteomic modules that strongly correlated with transcriptomic modules tB, tJ and tL were p8 and p9 (both enriched for pathways related to RNA splicing), and p12 (significantly enriched for the pathway “HDACs deacetylate histones”) (**Supplementary Table 4**). The latter is consistent with our earlier observations that a histone pathway signature was prominently associated with COVID-19 severity in both the RNA-seq (**Figure 3C**, **Supplementary Figure 6**) and plasma proteomic data (**Supplementary Figure 7C**).

In contrast to tB, tJ and tL, the other transcriptomic modules (tP, tC, tF, tI, tN) all displayed a decreasing trajectory in patients with worse disease (**Figure 4A**). These transcriptomic modules tended to be positively associated with imputed lymphocyte subset proportions and negatively associated with imputed myeloid proportions, implying that higher lymphocyte-related gene signatures and lower myeloid-related ones is a favourable prognostic sign (**Supplementary Figure 11**). While we cannot distinguish correlation from causation or indeed reverse causation, it is possible that these modules represent genes that enable an appropriate host response enabling viral clearance without an excessive inflammatory response.

#### Flow cytometry identifies markers of enhanced interferon signaling early in severe disease

To understand whether transcriptional signatures in PBMCs reflected changes in blood cell proportions, we performed flow cytometry on a subset of PBMC samples from the Wave 2 cohort. We found no major difference in the overall proportions of myeloid or lymphoid cells within the PBMC fraction between pre-infection and COVID-19 positive samples, except for a reduction in the proportion of type 2 dendritic cells (**Supplementary Figure 12**). Similarly,

there was little difference in the distribution of cells between mild/moderate and severe/critical patients. We observed some severity-related differences within cell subsets. Within lymphoid cells, we noted higher expression of the activation marker CD69 on CD4<sup>+</sup> T cells at day 7 in severe/critical disease compared to either pre-infection or mild/moderate disease (**Supplementary Figure 13A**). At day 14, there was an increase in CD38<sup>hi</sup> plasmablasts in severe/critical disease compared to pre-infection or mild/moderate samples (**Supplementary Figure 13B**). We also found that in severe/critical patients, there was a progressive drop in the proportion of non-classical monocytes over the first 14 days of the illness that was more marked than in mild/moderate patients (**Supplementary Figure 14A**). In severe/critical patients there was a greater proportion of intermediate and non-classical monocyte subsets expressing CD38 compared both to pre-infection samples and to mild/moderate patients (**Supplementary Figure 14B**), likely reflecting enhanced activation [30]. In classical monocytes there was a similar, but non-significant, trend. We found higher expression of proliferation-associated Ki67 on classical monocytes in COVID-19 versus pre-infection samples in both mild/moderate and severe/critical patients (**Supplementary Figure 14C**). In our transcriptomic data we identified increased *SIGLEC1* gene expression in COVID-19 (**Figure 2B**). SIGLEC-1 is exclusively expressed by CD14<sup>+</sup> monocytes at the protein level. SIGLEC-1 expression measured by flow cytometry correlated with GSVA enrichment score of type I IFN signatures (**Supplementary Figure 14D**). We observed SIGLEC1 expression increased at greater intensity as early as day 0-3 post infection in severe/critical versus mild/moderate patients, suggesting stronger and a more immediate type I IFN response in severe COVID-19 (**Supplementary Figure 14E**).

### Longitudinal cytokine/chemokine analysis reveals distinct temporal profiles that distinguish disease severity

Many plasma proteins associated with severe COVID-19 are canonically intra-cellular proteins. Their elevation in severe COVID-19 may therefore be a readout of increased cell turnover, death, stress, and viral hijacking of host cellular machinery. Consequently, we performed a more focussed analysis examining proteins whose primary biological role is to act extra-cellularly (e.g. cytokines, chemokines, growth factors and their receptors). These classes of proteins are important therapeutic targets in inflammatory diseases [32]. Accordingly, we modelled the temporal profiles of 232 proteins that fell within the KEGG pathway “Cytokine-cytokine receptor interaction”. Fifty proteins had significantly different profiles in patients with a severe/critical clinical course versus those with mild/moderate ones (TxCC interaction effect, 5% FDR; **Supplementary File 10**). Proteins exhibited distinct patterns of divergence between severe/critical and mild/moderate disease over time (**Figure**

5A). Some (e.g. IL1 $\beta$ , IL6, IL15RA, CCL2) showed a relatively stable temporal profile in mild/moderate patients but rising trajectories in severe/critical patients (**Figure 5B**). Others (e.g. CCL15, TNFSF13B (BAFF), PDGFRB, EDAR, IFNA10, IFNA13, IFNA16, IFNE and IFNL3) were elevated early in the disease course and decreased over time, but displayed more marked initial elevations in severe/critical patients (**Figure 5C**). Yet other proteins displayed temporal profiles in mild/moderate patients that were inverted compared to severe/critical. For example, CD40LG, TNFSF10 (TRAIL) and IL11 were reduced in the severe/critical versus the mild/moderate group at early timepoints but increased in severe/critical patients later (**Figure 5D**). Conversely, leptin, INHBA (inhibin A), and CCL22 were initially higher in severe/critical than mild/moderate patients but with the reverse pattern later on (**Figure 5E**). These data illustrate the dynamic nature of the soluble protein response and how this varies according to disease severity, highlighting the limitation of studies that use a single snapshot.

### Plasma LRRC15 as a predictor of COVID-19 severity

We next investigated whether clinical severity could be inferred from the transcriptomic and/or proteomic data and which had the better predictive performance. For this analysis, we combined the COVID-19 cases from both cohorts. For each COVID-19 patient, we selected the first sample at the patient's peak severity score so that there was one sample per patient. To predict COVID-19 severity at time of sampling, we employed two supervised learning methods, lasso and random forests. We applied these separately on i) the plasma proteomic data; ii) the PBMC transcriptomic data; and iii) the combination of both (the multi-omic data).

The proteomic-based models consistently outperformed the transcriptome-based ones, with non-overlapping 95% confidence intervals (**Figure 6A, Supplementary Figure 15A**). The lasso model generated on the proteome had an estimated area under the curve (AUC) of 0.93 (versus 0.86 for the transcriptome). The random forests model generated on the proteome had an AUC of 0.88 (versus 0.83 for the transcriptome). The models based on the proteome alone also had greater predictive performance than those trained on the multi-omic data, although the confidence intervals for the AUC estimates overlapped (**Figure 6A, Supplementary Figure 15A**).

We next examined the supervised learning models to identify the most important biomarkers of severe/critical disease (**Methods**) (**Figure 6B, Supplementary Figure 15B, Supplementary File 1P-R**). Although only a minority of the input features to the "multi-omic" model were proteins (34%; 6,323/18,548), proteins made up the majority of the top 15 most

important predictors (10/15 for lasso and 9/15 for random forests). This, and our finding that the plasma proteome was a superior predictor of severity than the PBMC transcriptome, highlights that plasma proteins provide a valuable read-out of the pathophysiological processes in severe COVID-19.

Importantly, both lasso and random forests identified plasma LRRC15 protein levels as the most important predictor of COVID-19 severity. Interestingly, this protein was recently identified by two pre-prints as a receptor for SARS-COV-2 [33,34]. We next examined LRRC15's longitudinal trajectory over the course of COVID-19 infection, finding that it displayed a different temporal profile dependent on the disease course ( $p < 0.0001$ , TxCC interaction, LMM). The concentration was stable in most individuals with mild/moderate COVID-19 (**Figure 6C**), whereas it decreased over time in severe/critical patients. Thus, a snapshot level of LRRC15 and its dynamic profile over time can convey information on the current clinical state of the patient and the overall course of the disease, respectively.

#### Persistent deranged platelet and coagulation pathways in convalescence

For 12 of the 17 patients in the Wave 2 cohort, we obtained a sample after clinical recovery at approximately two months following the acute infection. PCA analysis of the PBMC transcriptome showed that while pre-COVID-19 and convalescent samples appeared more similar than samples taken during COVID-19, there were differences between the convalescent samples and their pre-infection counterparts (**Figure 7A**), indicating that they have not fully returned to baseline. Comparison of the convalescent samples to their paired pre-COVID-19 samples revealed 25 significantly differentially expressed genes (1% FDR), of which 24 were up-regulated post-COVID-19 (**Figure 7B, Table 1, Supplementary File 1S**). Up-regulated clotting-related genes included *PF4* (encoding platelet factor 4) and the related gene *PF4V1* (platelet factor 4 variant 1). Of note, these genes are located in the same genomic region on chromosome 4, along with the chemokine *CXCL5*, which was also significantly up-regulated. Another nearby gene, *PPBP* (Pro-Platelet Basic Protein, aka *CXCL7*), was also up-regulated in convalescent samples, although it did not quite reach significance at 1% FDR (nominal  $P = 3.33 \times 10^{-5}$ , adjusted  $P = 0.0159$ ). The upregulation of these neighbouring genes suggests they are influenced by a shared genomic regulatory element. Overrepresentation analysis of the 25 differentially expressed genes revealed significant enrichment of terms including "Platelet activation, signaling and aggregation", "Formation of fibrin clot/clotting cascade", "Chemokine signaling pathway", "SARS-CoV-2 innate immunity evasion and cell-specific immune response" and "Smooth muscle contraction" (**Figure 7C, Supplementary File 1T**). These data suggest persistent activation of abnormal processes for a considerable

time after clinical recovery. In particular, they implicate the vascular and clotting systems, which may have implications for long-term risk of thrombosis.

## Discussion

This study leverages a unique feature of COVID-19 in patients with ESKD on haemodialysis: the possibility of obtaining serial blood samples throughout the disease course, irrespective of disease severity. This allows a rare insight into the pathogenesis of COVID-19 through examination of the temporal evolution of molecular and cellular changes. Moreover, ESKD patients are an important group to study as they are at substantial risk of severe or fatal disease [21,35]. Despite the remarkable success of vaccination programmes at the population level, ESKD patients display impaired vaccine responses [23,24]. In addition, the majority of patients in our study were of non-white ethnicity, which is also a risk factor for severe disease [21].

Most studies of circulating proteins in COVID-19, including our previous work, have used Olink immunoassay technology [8–10] or mass spectrometry [11,12]. The broadest Olink assay system, used in the study of Filbin et al [8], measures 1,472 proteins, while mass spectrometry is generally limited to reliable detection of less than 1,000 plasma proteins and lacks sensitivity for low abundance proteins. A small number of studies have employed the aptamer-based SomaScan v4 platform, that measures 4,665 unique proteins [8,13–16]. Here, we used the SomaScan v4.1, which measures 6,323 unique proteins, and complemented this with RNA-seq and flow cytometry. Our study is strengthened by data from two cohorts from different waves of the pandemic, and the comparison of samples from before, during and after COVID-19 from the same individuals.

Plasma proteomics identified several pathways upregulated in COVID-19 related to host defence against viruses, including those previously described in SARS-CoV-2. Our PBMC transcriptomic analysis identified numerous pathways that are up-regulated in COVID-19. Many have been identified in previous studies of COVID-19 in other populations without ESKD, indicating the presence of common patterns of COVID-19-related immunological abnormalities. Examples include type 1 interferon signaling, the complement cascade, and genes reflecting leukocyte-vascular interactions. Other up-regulated pathways included “Polo-like kinase mediated events” and “Golgi-cisternae peri-centriolar stack re-organisation”. Both are likely to reflect the extensive cell division of immunocytes that occurs in COVID-19. For instance, the pericentriolar stacks of Golgi cisternae undergo extensive fragmentation and reorganization in mitosis. Similarly, polo-like kinase is crucial for facilitating the G2/M

transition. These findings are consistent with the up-regulation of APC-Cdc20 mediated degradation of Nek2A and other APC-Cdc20 related processes that we observed in the proteomic data; Cdc20 is a protein that is key to the process of cell division.

Transcriptomic and proteomic associations with severe COVID-19 converged on some unifying themes. For example, up-regulation of histone-encoding genes and elevated plasma histone protein levels were both markers of COVID-19 severity. The increased expression of histone-encoding transcripts may indicate increased immune cell proliferation. In each cell cycle, sufficient histones are needed to package the newly replicated daughter DNA strands, requiring tight coupling of histone synthesis to the cell cycle [36]. Excess histones within cells can trigger chromatin aggregation and block transcription [37]. Thus, in severe COVID-19, viral hijacking of cellular machinery may contribute to cellular damage through decoupling of DNA synthesis and histone transcription. The preponderance of plasma histone proteins in severe disease is likely to reflect the higher levels of cell damage and death. The presence of histone proteins in plasma, however, is likely to represent more than just a marker of disease. Histones are constituents of neutrophil extracellular traps (NETs) which contribute to tissue injury in severe COVID-19. In addition, histones constitute powerful damage associated molecular patterns (DAMPs) and can perpetuate inflammation via ligation of toll-like receptors and direct damage to epithelial and endothelial cells [38]. Upregulation of pathways related to control of transcription and translation was another feature of severe COVID-19 (**Supplementary Figure 7B**), perhaps reflecting subversion of normal cell biology by SARS-CoV-2. In keeping with this, studies of cells infected with SARS-CoV-2 revealed “re-shaping” of processes including translation, splicing and nucleic acid metabolism [39,40].

Modular analysis highlighted a rising neutrophilic gene signature as the illness progressed in severe/critical patients, with enrichment of reactive oxygen and nitrogen species pathways. This suggests prolonged activation of neutrophils and their key effector pathways including NET formation. This neutrophilic gene signature likely indicates the presence of low-density granulocytes within the PBMC fraction. Data from other infections suggest that phagocyte NADPH oxidase-derived reactive oxygen species can be detrimental in acute viral infection; mice lacking components of the NADPH oxidase have reduced disease severity and inflammation in response to influenza and lymphocytic choriomeningitis virus infection [41][42][43].

Cytokines and their receptors play a major role in the pathogenesis of inflammatory diseases and are important targets of existing drugs [32]. Longitudinal examination of plasma cytokines/chemokines revealed divergence temporal trajectories between disease severity

strata, manifesting in several patterns (**Figure 5**). For example, in patients with a severe/critical disease course, IL11 was reduced early on but increased later relative to more indolent disease (**Figure 5D**). IL11 is known to cause progressive fibrosis [44,45], and the marked increases late in severe/critical disease may have implications for the development of pulmonary sequelae. Leptin, INHBA (inhibin A), and CCL22 showed the opposite pattern (**Figure 5E**). Leptin has roles in both cell metabolism and immunity with many immune cells responding to leptin directly via the leptin receptor, resulting in a pro-inflammatory phenotype [46]. It is produced by adipocytes, so its elevation early in severe/critical disease may be a read-out of higher body mass index, which is a risk factor for severe COVID-19, or increased cell metabolism/turnover. Its fall over time in severe/critical patients may reflect weight loss and cell death. Whether leptin is also directly influencing risk of severe disease through its immunological effects is unclear. Inhibin-A progressively increased over time in mild/moderate patients but fell in severe/critical patients. Inhibin-A negatively regulates dendritic cell maturation and promotes a tolerogenic phenotype [47]. Failure to upregulate it later in the disease course may therefore contribute to deleterious inflammation. Similarly, CCL22 plays an important role in switching off inflammation. CCL22 promotes dendritic cell-regulatory T cell interactions and CCL22 deficiency is associated with excessive pathogenic inflammation in mice [48].

Proteins in the type 1 interferon (IFN) pathway were higher in severe/critical than mild/moderate patients early in disease (**Figure 5C**), suggesting a paradoxical role of this pathway in COVID-19. While inherited or acquired deficiencies of IFN proteins predispose to risk of severe COVID-19 [49,50], our data suggest that the picture may be more complex. Thus, IFNs may act as a double-edged sword, with harm to the host from both insufficient responses (leading to failure to control the virus) and from excessive responses (resulting in immunopathology). While we cannot exclude the possibility that increased IFNs is a consequence rather than a cause of severe disease, their elevation very early in disease suggests this is less likely. Another consideration is that the greater IFN response in severe disease might reflect higher viral burden.

Using two distinct supervised learning methods, we observed that the plasma proteome better captures disease severity than the PBMC transcriptome. When supervised learning algorithms were trained on both the proteomic and transcriptomic data simultaneously, plasma proteins dominate the list of important biomarkers. There are several reasons why this might be the case. Plasma is under strong homeostasis: derangement is a marker of loss of physiological control. Plasma proteins may provide important read-outs of both pathogenesis and tissue

injury by reflecting the activity of cell types other than PBMCs, such as neutrophils, endothelium and hepatocytes (a major source of coagulation and complement proteins).

A striking finding was the predictive value of plasma levels of LRRC15 in indicating COVID-19 severity. Longitudinal profiling revealed that LRRC15 levels remain stable in those with a mild/moderate clinical course but decrease over time in severe/critical illness (**Figure 6C**). Our findings are particularly intriguing as two recent pre-prints have identified LRRC15 as an accessory factor for SARS-CoV-2 entry to cells. Using arrayed transmembrane protein and pooled genome-wide CRISPR activation screens, Shilts and colleagues demonstrated that the SARS-CoV-2 spike protein interacts with LRRC15 [33]. Both screens identified the interaction and the CRISPRa screen identified LRRC15 and the established SARS-CoV-2 binding partner, ACE2, as the two most prominent interactors. This work also showed that ACE2 and LRRC15 bind the C-terminal domain of the spike protein, which contains the receptor binding domain, suggesting that the two proteins may compete for spike protein binding. Song and colleagues also used a CRISPRa approach to identify proteins that could bind the SARS-CoV-2 spike protein to the A375 melanoma cell line [34]. The screen identified ACE2 and LRRC15, and further showed that the interaction took place with the receptor binding domain of the spike protein. Expression of LRRC15 on a HeLa cell line that expresses ACE2 inhibited the entry of a SARS-CoV-2 spike pseudovirus. This paper notes, however, that LRRC15 is expressed on different cells from those that express ACE2 and proposes that LRRC15 inhibits virally entry *in trans*, acting as a decoy and binding virions that cannot then enter cells via ACE2. Our data are consistent with a model in which a failure to up-regulate LRRC15 increases risk of severe COVID-19 disease because of the lack of a receptor that inhibits its entry to cells. Thus our study is the first human *in vivo* study to highlight the importance of LRRC15 in the response to SARS-CoV-2.

Another unique strength of our study was the availability of baseline pre-infection samples for the Wave 2 cohort, as well as samples taken two months after the acute COVID-19 episode. Leveraging this, we demonstrate that there is chronic activation of vascular, platelet and coagulation pathways for a prolonged period after clinical resolution of disease. The elevated risk of thrombotic events during acute COVID-19 is well-documented. In a large study encompassing both hospitalised and non-hospitalised patients [51], the risk of pulmonary embolism (PE) and deep vein thrombosis (DVT) were 27-fold and 17-fold increased, respectively, in the seven days following diagnosis. These risk ratios are much higher than those previously associated with upper respiratory tract infections, suggesting unique features specific to SARS-CoV-2 infection. The risk of arterial thrombosis was also significantly increased, although smaller in magnitude than the risk of venous thromboembolism (VTE).

The pathophysiology underlying COVID-19 associated coagulopathy is complex and involves the convergence of several pathways [52]. Invasion of ACE2-expressing epithelial cells by SARS-CoV-2 results in down-regulation of ACE2 and increased angiotensin II levels. This in turn leads to increased expression of PAI1 which impairs breakdown of fibrin and promotes increased vascular tone, via smooth muscle contraction. Endothelial cell activation, complement activation, NETosis, hypoxia and cytokine/chemokine secretion all promote coagulopathy through increases in tissue factor and concomitant fibrin formation. Remarkably, our data suggest that these pathways remain dysregulated months after acute infection has resolved (**Figure 7, Table 1**). This is particularly important given emerging evidence indicating that the risk of thrombo-embolism extends beyond the acute phase. Ho *et al* showed that risk of a PE was 3.5-fold higher even in the time window 28 to 56 days after diagnosis of COVID-19 [51]. A recent population-wide registry study revealed that following COVID-19 the risk of DVT and PE was significantly elevated for 70 and 110 days, respectively [53]. Although VTE risk was greatest for those with severe disease, even patients with mild disease had elevated VTE risk. Our data provide a molecular basis that begins to explain this risk. Intriguingly, among the genes up-regulated in convalescent samples compared to pre-infection was platelet factor 4 (*PF4*). *PF4* is expressed in platelets and leucocytes. It is released from the alpha granules of activated platelets, contributing to platelet aggregation. The prolonged up-regulation of *PF4* after COVID-19 is therefore likely to contribute to a prothrombotic state. Of note, autoantibodies to *PF4* are the pathogenic entity in both vaccine-induced thrombotic thrombocytopenia (VITT) [54,55] and heparin-induced thrombocytopenia (HIT). *PF4* becomes an autoantigen when it forms complexes with adenoviral vaccine components or heparin respectively, unmasking epitopes to which autoantibodies bind [56]. It will therefore be interesting for future studies to investigate whether autoantibodies to *PF4* might contribute to post-COVID-19 thrombosis in some patients. Whether the molecular abnormalities found in our study also apply to more general patient populations without background ESKD needs to be determined. Ongoing studies focusing on the sequelae of COVID-19 are well placed to address this.

Our study has several limitations. ESKD patients have considerable multi-morbidity and deranged physiology, and our findings may not all be generalisable to other patient populations. We lacked a comparator group of ESKD patients with another viral infection to delineate COVID-19 specific features. We studied peripheral blood; while this can provide valuable information, it does not always reflect processes at the site of tissue injury. We performed bulk RNA-seq on PBMCs. Thus, transcriptomic signatures may reflect both changes in gene expression and also alteration in the distribution of cell subtypes within PBMCs. We mitigated this issue through use of deconvolution methods and flow cytometry,

but future studies using single cell RNA-seq and CITE-seq will provide further granularity. We did not have measurements of viral load which would have aided interpretation of the magnitude of host responses (e.g. interferon signaling). Finally, the convalescent samples were taken relatively soon after clinical recovery: it will be important for future studies to establish how long molecular abnormalities persist.

In summary, we demonstrate dynamic transcriptomic, proteomic and cellular signatures that vary both with time and COVID-19 severity. We show that in patients with a severe clinical course there is increased type 1 interferon signaling early in the illness, with increases in pro-inflammatory cytokines later in disease. We identify plasma levels of the proposed alternative SARS-CoV-2 receptor, LRRC15, as the strongest predictor of COVID-19 severity. Finally, we show that immune cells display dysregulated gene expression two months following COVID-19, with upregulation of clotting-related genes. This may contribute to the prolonged thrombotic risk post-COVID-19.

## Methods

### Patient cohorts and ethical approval

All participants (patients and controls) were recruited from the Imperial College Renal and Transplant Centre and its satellite dialysis units, London, United Kingdom, and provided written informed consent prior to participation. Study ethics were reviewed by the UK National Health Service (NHS) Health Research Authority (HRA) and Health and Care Research Wales (HCRW) Research Ethics Committee (reference 20/WA/0123: The impact of COVID-19 on patients with renal disease and immunosuppressed patients). Ethical approval was given.

We recruited two cohorts of ESKD patients with COVID-19 (**Figure 1A**). All patients were receiving haemodialysis prior to acquiring COVID-19. The first cohort ('Wave 1') were recruited during the initial phase of the COVID-19 pandemic (April-May 2020). Blood samples were taken from 53 patients with COVID-19 (**Supplementary Table 1**). Serial blood sampling was carried out where feasible (**Figure 1B**), given the pressure on hospital services and the effects of national lockdown. We also contemporaneously recruited 59 non-infected haemodialysis patients to provide a control group, selected to mirror the age, sex and ethnicity distribution of the COVID-19 cases (**Supplementary Figure 1A-C**).

The Wave 2 cohort consisted of 17 ESKD patients with COVID-19 infected during the resurgence of cases in January-March 2021 (**Supplementary Table 2**). These 17 individuals had all been recruited as part of the COVID-19 negative control group during Wave 1, and so a pre-infection sample collected in April/May 2020 (8-9 months preceding infection) was also available. For the Wave 2 cohort, we systematically acquired serial samples for all patients at regular intervals (every 2-3 days over the course of the acute illness) (**Figure 1C**). Additionally, for 12 of these 17 patients, we acquired convalescent samples at approximately 2 months post the acute COVID-19 episode (range 41-55 days from the initial sample). Convalescent samples were unavailable for four patients who died and for one patient due to logistical difficulties in sample collection.

To minimise variation related to the timing of dialysis, blood samples were taken prior to commencing a haemodialysis session.

## Clinical severity scoring

We assessed disease severity using a four-level ordinal score, categorising into mild, moderate, severe, and critical, based on the WHO clinical management of COVID-19: Interim guidance 27 May 2020. 'Mild' was defined as COVID-19 symptoms but no evidence of pneumonia and no hypoxia. 'Moderate' was defined as symptoms of pneumonia or hypoxia with oxygen saturation (SaO<sub>2</sub>) greater than 92% on air, or an oxygen requirement no greater than 4 L/min. 'Severe' was defined as SaO<sub>2</sub> less than 92% on air, or respiratory rate more than 30 per minute, or oxygen requirement more than 4 L/min. 'Critical' was defined as organ dysfunction or shock or need for high dependency or intensive care support (i.e. the need for non-invasive ventilation or intubation). We recorded disease severity scores throughout the illness, such that samples from the same individual could have differing severity scores according to the temporal evolution of the disease. We defined the overall clinical course for each patient as the peak severity score that occurred during the patient's illness. Different downstream analyses utilise either the severity at the time of sample (i.e. the sample-level severity) or the overall clinical course (i.e. the patient-level severity), as described in the relevant sections below.

## PBMC collection protocol

Peripheral blood mononuclear cells (PBMCs) were obtained by density gradient centrifugation using Lymphoprep (STEMCELL Technologies, Canada). Approximately 20 ml of blood were diluted 1x with phosphate buffered saline (PBS) with addition of 2% FBS and layered on top of 15 ml of Lymphoprep solution. The samples were then centrifuged at 800 g for 20 minutes at room temperature without break. PBMCs were collected from the interface and washed twice with PBS/2%FBS. 2 million PBMCs were centrifuged down to form a pellet and resuspended in 350 µl RLT buffer + 1% β-Mercaptoethanol (from Qiagen RNeasy kit) for RNA extraction. Remaining PBMCs were cryopreserved in 1 ml freezing medium (FBS 10% DMSO) and stored in -80 degrees C freezer.

## Plasma collection.

5 ml of blood was collected in EDTA tubes and centrifuged at 1000 RPM for 15 mins. Plasma was extracted and frozen at -80 degrees Celcius.

## RNA-seq of PBMCs

RNA extraction and sequencing were done at GENEWIZ facilities (Leipzig, Germany). Total RNA was extracted from using RNeasy Mini kits (Qiagen) as per the manufacturer's instructions, with an additional purification step by on-column DNase treatment using the RNase-free DNase Kit (Qiagen) to remove any genomic DNA. Total RNA quality and concentration was analysed using Agilent Tapestation (Agilent Tech Inc.). Samples with RIN values ≥ 6.0 and ≥ 100 ng of total RNA were used to generate RNA-seq libraries. RNA-seq libraries were made using NEBnext ultra II RNA directional kit per the manufacturer's instruction. Poly-A RNA was purified using poly-T oligo-attached magnetic beads followed by hemoglobin mRNA depletion using QIAseq FastSelect Globin Kit to remove potential contaminating RNA from red blood cell. Then, first and second cDNA strand synthesis was performed. Next, cDNA 3' ends were adenylated and adapters ligated followed by library amplification. The libraries were size selected using AMPure XP Beads (Beckman Coulter), purified and their quality was checked using a short sequencing run on MiSeq Nano. Samples were randomized to avoid confounding of batch effects with clinical status and multiplexed libraries were run on 29 lanes of the Illumina HiSeq platform to generate approximately 30 million x 150bp paired-end reads per sample.

Initial quality control and alignment was performed using the nf-core RNA-seq v3.2 pipeline [57] based on nextflow [58], a workflow management system. FastQC [59] was used to evaluate and merge paired reads prior to adapter trimming using Trimalore [60]. We used STAR [61] to align reads to GRCh38 and htseq-count [62] to generate a counts matrix.

For the Wave 1 cohort, following quality control (QC), transcriptomic data were available for 179 samples from 51 COVID-19 positive ESKD patients (median 3 samples per patient, range 1-8) (**Supplementary Figure 1D**), plus 55 non-infected ESKD patient samples. For the Wave 2 cohort (17 patients), following QC, transcriptomic data were available for 90 samples collected during acute COVID-19 infection (median of 6 samples per patient, range 3-7), plus 17 pre-infection samples and 12 convalescent samples.

Prior to further analysis, genes with insufficient counts were removed using edgeR's filterByExpr function [63]; for differential expression analyses, the "group" argument was set to the main group of interest. For all analyses, gene expression was TMM normalised [64], converted to counts per million (CPM) and log-transformed. We primarily used ENSEMBL identifiers [65], however for plots we report the HGNC gene ID [66] where available. For analyses that considered multiple proteins simultaneously (PCA, WGCNA, MEFISTO, supervised learning), we additionally: i) removed genes with low variance (33% of genes with the lowest maximum absolute deviation) [67]; ii) centered and scaled the data.

### Plasma proteomics

We performed proteomics on EDTA plasma samples using the aptamer-based SomaScan platform (Somalogic, Boulder, Colorado, USA). The SomaScan v4.1 assay contains 7,288 modified-aptamers (Somamers) that target human proteins. Since more than one aptamer may target the same protein, these 7,288 aptamers map to 6,347 unique proteins. 48 Somamers were removed due to QC failure, so the final dataset contains 7,240 Somamers representing 6,323 unique proteins. We annotated these proteins using the Human Protein Atlas [68]; 4,980 proteins were labelled as intracellular, 1,586 were annotated as membrane proteins and 1,160 as secreted (**Supplementary Figure 16A**). Many proteins were labelled as both intracellular and as membrane or secreted, reflecting the biology of protein storage and extra-cellular secretion/excretion (**Supplementary Figure 16B**).

We report proteins by their corresponding HGNC gene ID [66], which provides a more standardised nomenclature compared to protein names and allows direct comparison with the transcriptomic data.

Where multiple Somamers related to the same protein, we retained these Somamers for univariate analyses such as differential abundance analyses. However, for analyses that considered multiple proteins simultaneously (PCA, WGCNA, MEFISTO, supervised learning), we selected one Somamer at random to represent each protein. One COVID-19 positive sample in the wave 2 cohort failed QC and was excluded from the analyses. The raw SomaScan data was separated by cohort. The expression values for each Somamer were inverse-rank normalised prior to downstream analyses.

For the Wave 1 cohort, following QC, proteomic data were available for 86 samples from 37 COVID-19 positive ESKD patients (median 3 samples per patient, range 1-3), plus 53 non-infected ESKD patients. For the Wave 2 cohort (n=17 patients), following QC, proteomic data were available for 102 samples collected serially during acute COVID-19 infection (median of 6 samples per patient, range 5-7) and 16 pre-infection samples.

### Differential expression analyses: COVID-19 positive versus negative

We compared COVID-19 positive and negative patients using linear mixed models (LMM), which account for serial samples from the same individual [69]. Age, sex and ethnicity were included as covariates. A random intercept term was used to estimate the variability between individuals in the study and thus account for repeated measures. We performed differential expression analyses for the transcriptomic data and the proteomic data. The regression model for these analyses in Wilkinson-style notation was:

$$E \sim \text{covid\_status} + \text{sex} + \text{age} + \text{ethnicity} + (1 \mid \text{individual})$$

where, E represents expression (gene or protein, depending on the data type being analysed) and “covid\_status” was a categorical variable (infected/non-infected).

For differential expression of proteins, we applied LMM using the lmerTest package [70]. Differential gene expression analysis was performed using the same model formula, applied using the differential expression for repeated measures (dream) pipeline [71] in the variancePartition package [72]. For all data types, we fitted LMM using restricted maximum likelihood (REML) and calculated P-values using a type 3 F-test, in conjunction with Satterthwaite’s method for estimating the degrees of freedom for fixed effects [70]. Multiple testing correction was performed using the Benjamini-Hochberg method and a 1% FDR used for the significance threshold.

The Wave 1 cohort was analysed separately to the Wave 2 cohort. For Wave 1, we compared samples from COVID-19 positive ESKD patients to COVID-19 negative ESKD patients. For Wave 2, we compared samples from COVID-19 positive ESKD patients to samples from these patients taken approximately 8 months prior to infection.

When reporting the number of differentially expressed proteins in the text we refer to the number of unique proteins rather than the number of significant Somamers.

### Testing transcriptomic and proteomic features for association with COVID-19 severity

We performed a within-cases analysis, testing for the association of gene expression with COVID-19 severity at time of sampling. We used the four-level WHO severity rating (mild, moderate, severe, critical), which could vary between samples from the same individual reflecting the clinical status at the time the sample was taken. We again used a linear mixed model to account for samples from the same individual. The regression model was:

$$E \sim \text{covid\_severity} + \text{sex} + \text{age} + \text{ethnicity} + (1 \mid \text{individual})$$

The “covid\_severity” variable represents severity at the time of the sample and was encoded using orthogonal polynomial contrasts to account for ordinal nature of severity levels.

COVID-19 positive samples from the Wave 1 cohort were analysed separately to those from the Wave 2 cohort.

The same approach was used for the proteomics data.

### Gene set variation analysis

To identify pathways that were up- or down-regulated in COVID-19 positive versus negative samples, we applied gene set variation analysis (GSVA) [25]. To define gene sets, we used the MSigDb C2 canonical pathways [73]; we discarded sets with less than ten genes. We additionally included a gene set for the peripheral immune response defined for patients with severe COVID-19 [26] and a set of type 1 interferons active in patients with systemic lupus erythematosus (SLE) [74]. After reduction of genes into gene sets, we then performed testing for dysregulated pathways using the same linear mixed modelling approach as for the differential gene and protein expression analyses. P-values were adjusted by Benjamini-Hochberg, with a significance threshold of 1% FDR.

To dissect out the key molecules underpinning enriched pathways, we examined the genes that comprise these pathway terms and identified which of these featured most prominently in the differential gene expression analysis.

We repeated this procedure for testing of association of pathways with severity at the time of sample using the 4-level ordinal score.

We then applied the same approach to the proteomics data for the COVID-19 positive versus negative analysis, and for testing associations with COVID-19 severity at the time of sample.

### **Robust rank aggregation**

The Wave 1 and Wave 2 cohorts were analysed separately for both the differential expression analyses between COVID-19 positive and negative samples and for the within-cases severity analyses. To identify the associations that were most consistent between the Wave 1 and Wave 2 cohorts, for each analysis, we integrated the P-values for each cohort using robust rank aggregation (RRA) [75]. This method identifies features that are ranked higher than expected across multiple lists. RRA generates a significance score analogous to a P-value; we  $-\log_{10}$  transform these values such that a larger score indicates more consistent associations between the Wave 1 cohort and the Wave 2 cohort. RRA was applied to the results of the transcriptomic, proteomic and GSVA analyses comparing COVID-19 positive versus negative samples from Wave 1 and Wave 2. Similarly, it was applied to the analyses testing for association of molecular features with COVID-19 severity at the time of sampling.

### **Modelling modular longitudinal trajectories**

We examined the temporal trajectories of the transcriptome following infection, by explicitly modelling molecular markers with respect to time following COVID-19 symptom onset. We used a two-step approach.

Step 1. To aid biological interpretation, we first applied a dimension reduction strategy using weighted gene correlation network analysis (WGCNA) [29] to identify modules of correlated molecular features. For this analysis, we combined samples from the Wave 1 and Wave 2 cohorts. Additionally, since our goal was to perform longitudinal analysis, we only selected patients who had been sampled at least three times prior to 21 days following COVID-19 symptom onset. The default implementation of WGCNA is not designed for use with non-independent samples [76], so we modified the analysis pipeline by generating a correlation matrix using a repeated measures correlation metric (rmcorr) that is appropriate for repeated measures [77]. We used WGCNA's `pickSoftThreshold.fromSimilarity` function to pick the minimum soft-thresholding power that satisfied the minimum scale free topology fitting index ( $R^2 > 0.85$ ) and maximum mean connectivity (100). We subsequently defined signed adjacency and topological overlap matrices before applying average-linkage hierarchical clustering. We cut this tree with a hybrid dynamic tree cutting algorithm, with the parameters `deepSplit = 4` and `minClusterSize = 30` [78]. Finally, we defined eigengenes for each module and merged those with a distance less than 0.25. The eigen-genes provide a numerical representation for each module of co-expressed genes.

We used the same approach to analyse the proteomic data.

Step 2. To examine the trajectory of each module over time, we fitted a linear mixed model with time from symptom onset as an independent variable and the eigengene (or eigenprotein in the case of proteomic modules) as the dependent variable. Time was defined for each sample as time from first symptoms; where date of first symptoms was not available, we instead used date of first positive swab. Samples that were taken more than 21 days from each individual's baseline date were excluded. We used R's `bs` function to fit a polynomial spline of degree two to model the expression of modules with respect to time from baseline [79]. To test whether modules displayed different temporal patterns according to the overall clinical course of COVID-19 (defined as a binary variable indicating whether the peak WHO severity score was mild/moderate or severe/critical), we included clinical course as a covariate in the model, and an interaction term between time from symptom onset and clinical course (TxCC).

The regression model used is displayed using Wilkinson-style notation below.

eigen-expression ~ clinical\_course \* time + sex + age + ethnicity + wave + (1 | individual)

We extracted the P-values for the TxCC term in this model and applied Benjamini-Hochberg adjustment, using 5% FDR as the significance threshold. A significant interaction effect for the TxCC term indicates that the module has a different temporal profile in mild/moderate versus severe/critical disease.

### **Additional WGCNA module annotation and association testing**

To better understand the biological information reflected in the transcriptomic and proteomic modules, we further characterised them through a multi-pronged analytical strategy. We tested association of eigen-genes and eigen-proteins with other variables. First, we tested for the association of the modules with WHO severity at the time of the sample using the LMM approach described above in subsection ‘Testing transcriptomic and proteomic features for association with COVID-19 severity’ i.e.:

$$E \sim \text{covid\_severity} + \text{sex} + \text{age} + \text{ethnicity} + \text{wave} + (1 | \text{individual})$$

Second, since PBMCs represent a mixed population of immune cells, we investigated whether disease trajectory-associated transcriptomic modules might reflect shift in cell type proportions. To this end, we applied CIBERSORTx, a computational algorithm to impute immune cell fractions from RNA-seq data (see subsection ‘Cell fraction imputation’ below). We then tested for correlations between these imputed immune cell proportions and module eigengenes using LMM:

$$\text{eigen-expression} \sim \text{cell\_fraction} + \text{sex} + \text{age} + \text{ethnicity} + \text{wave} + (1 | \text{individual})$$

Both these models included an additional fixed effect (“wave”) to reflect the cohort.

Third, we performed pathway enrichment analysis on the modules using the R package clusterProfiler’s “enricher” function [80]. Gene sets were defined using MSigDB C2 canonical pathways [73].

Lastly, to understand the relationship between the transcriptomic and proteomic modules, we performed correlation analysis using LMM.

5% FDR was used for statistical significance for these analyses.

### **Cell fraction imputation**

We used CIBERSORTx [81] to impute cell fractions from the normalised bulk RNA-seq dataset. The program was run with default parameters We inferred the cell fractions of 22 immune cell types in the isolated PBMCs of each sample using the LM22 signature matrix file [82].

### **Multi-omic longitudinal factor analysis with MEFISTO**

MEFISTO [83] is an extension of Multi-Omics Factor Analysis (MOFA) that can exploit temporal relationships between samples to find factors that change over time (from baseline). We used this method to find joint factors of variation in the transcriptomic and proteomic datasets. For the MEFISTO analysis, we used the same set of samples as in the network analysis and applied the same pre-processing steps to the data (see **Methods – network analysis**). Additionally, we removed genes with the lowest maximum absolute deviation [67] such that the number of genes retained were equal to the number of unique proteins measured (6,323) to avoid imbalance numbers of features between the transcriptomic and proteomic data which can impact the MEFISTO algorithm. Using the “slow” convergence criterion,

MEFISTO identified 8 factors that had a minimal variance explained of 1% in at least one data modality.

We then applied the longitudinal model described earlier to test for an interaction effect between time from first symptoms and clinical course, with a latent factor identified by MEFISTO as the dependent variable. The regression model used is displayed using Wilkinson-style notation below:

$$\text{Latent\_factor} \sim \text{clinical\_course} * \text{time} + \text{sex} + \text{age} + \text{ethnicity} + \text{wave} + (1 | \text{individual})$$

### Longitudinal modelling of cytokines and cytokine receptors

We modelled the temporal profiles of 232 plasma proteins that fell within the KEGG pathway “Cytokine-cytokine receptor interaction”. As for the longitudinal analyses described earlier, we used a linear mixed model with a time x clinical course interaction term.

$$P \sim \text{clinical\_course} * \text{time} + \text{sex} + \text{age} + \text{ethnicity} + \text{wave} + (1 | \text{individual})$$

P values for the time x clinical course interaction were extracted and adjusted for multiple testing with the Benjamini-Hochberg procedure, with significance threshold of 5% FDR.

### Supervised learning

The goal of this analysis was to predict clinical severity from the molecular features (transcriptomic, proteomic or both). We performed supervised learning using the R caret framework [84]; caret uses the randomForest package to fit random forest models and glmnet [85] to fit lasso models. For this analysis, we only included samples on which both transcriptomics and proteomics had been performed. We then selected the earliest sample for each individual at which they had reached their peak COVID-19 WHO severity score, so that there was one sample per patient. We then categorised the clinical severity score corresponding to each sample into a binary variable such that patients with a WHO severity score of mild or moderate were considered “mild/moderate” and those with a WHO score of severe or critical were considered “severe/critical”. This resulted in n=37 mild/moderate samples and n=14 severe/critical samples.

We trained models using Monte Carlo cross-validation for: i) the plasma proteomic data alone (6,323 features); ii) the PBMC RNA-seq data alone (12,225 features); and iii) the combined proteomic and RNA-seq datasets. The first step in this training process was to create 200 random partitions of the data, such that 80% of the data was used to train the model in each resample and 20% was retained as a validation set. In each resample, we calculated the area under the curve (AUC) of the receiver operating characteristic (ROC) curve. We then calculated confidence intervals for the 200 AUC-ROC values generated for each model and feature type.

The random forest model’s parameters were kept constant at 500 trees and the mtry value (number of proteins randomly sampled as candidates at each node) was calculated as the square root of the number of features. After cross-validation, we fitted a final random forest model using the entirety of the dataset. We extracted important features from this model using the R randomForestExplainer package, based on the accuracy decrease metric (the average decrease in prediction accuracy upon swapping out a feature). For the lasso model, the lambda value that maximised the mean AUC-ROC during cross-validation was selected. We recorded the features selected by the lasso model in each data resample; feature importance was subsequently defined as the number of models in which each feature had a non-zero coefficient. The feature importance metrics from both models were scaled by dividing their values by the maximum value, such that the most important feature has an importance metric of 1.

## Differential gene expression analysis: pre-infection versus recovery samples

For the 12 individuals in the Wave 2 cohort for whom we collected a convalescent sample (approximately 2 months post-infection; range 41-55 days from the initial sample), we performed a differential gene expression analysis comparing these samples to the paired pre-infection samples using LMM, implemented with the R dream package [71]. Age, sex and ethnicity were included as covariates and a random intercept term used to account for the paired nature of the samples. Statistical significance was defined as 1% FDR. To identify enriched pathways in the list of differentially expressed genes, we performed overrepresentation analyses using the same approach as described above for annotating the WGCNA modules.

## Flow cytometry

Flow cytometry analysis was performed on a subset of the Wave 2 PBMC samples. We examined samples taken during acute COVID-19 from 17 patients (of whom 9 patients had a mild/moderate clinical course and 8 patients with severe/critical course), and pre-infection samples from 15 of these same patients.

Cryopreserved PBMCs were thawed in humidified 37°C, 5% CO<sub>2</sub> incubator and resuspended in thawing medium (RPMI, 20% FBS). PBMCs were washed twice with PBS and stained with Zombie Yellow LIVE/DEAD (Biolegend) following the manufacturer's protocol to exclude dead cells. Then, PBMCs were washed twice with FACS buffer (1% BSA, 0.09% Azide, 1 mM EDTA), and Fc receptors were blocked with Human TruStain Fc Receptor Blocking Solution (Biolegend). Then, surface staining were performed using the selected fluorochrome-conjugated monoclonal antibodies detailed in **Supplementary Table 5** for 20 minutes at 4°C. Following incubation, cells were fixed and permeabilized using the eBioscience™ Foxp3 / Transcription Factor Staining Buffer Set (Invitrogen) for intracellular staining. Cells were incubated with selected antibodies or isotype controls for 30 minutes at 4°C and resuspended in FACS buffer for analysis. Aurora Spectral Flow Cytometry (Cytek®) and FlowJo software, version 10 (Tree Star Inc. Ashland, OR, USA) were used for analysis of all samples.

## Flow cytometry statistical analysis

To evaluate decomposition performance by CIBERSORTx analysis, cell proportion estimates were compared to cell percentages from Flow Cytometry analysis using Pearson's correlation analysis (n=68 samples). We were unable to examine for the presence of LDGs using our flow cytometry data since this was performed on cryopreserved PBMCs and LDGs do not survive the freeze-thaw process (whereas we performed transcriptomics on RNA extracted from fresh PBMCs). We observed significant correlation of estimated cell proportions from CIBERSORTx analysis compared to proportions measured by flow cytometry for all other cell types (Pearson  $r > 0.4045$ ,  $p\text{-value} < 0.0001$ ).

For severity analysis, one sample per patient was selected at a time that coincided with the expected spike in the inflammatory response (nearest sample to day 7 after symptom onset; no more than +/- 72 hours). Patients were classified according to the overall peak illness severity into two groups (mild/moderate = 9, severe/critical = 8). Change of cell proportion across time were accessed by grouping samples into 4 days interval post COVID-19-positive test. One-way ANOVA was used to calculate significant differences between multiple groups with Dunnet's correction for multiple-way comparisons. Significance is based upon  $p\text{-value} < 0.05$ .

## Data and code availability

- Individual-level data for transcriptomics, proteomics and flow cytometry are available without restriction from Zenodo (doi: 10.5281/zenodo.6497251)
- Code is available at: <https://github.com/jackgisby/covid-longitudinal-multi-omics>

## Acknowledgements

The authors thank the patients who volunteered for this study and the staff at Imperial College Healthcare NHS Trust (the Imperial College Healthcare NHS Trust renal COVID-19 group and dialysis staff):

Appelbe M, Ashby DR, Brown EA, Cairns T, Charif R, Condon M, Corbett RW, Duncan N, Edwards C, Frankel A, Griffith M, Harris S, Hill P, Kousios A, Levy JB, Loucaidou M, Lightstone L, Liu L, Lucisano G, Lynch K, Mclean A, Moabi D, Muthusamy A, Nevin M, Palmer A, Parsons D, Prout V, Salisbury E, Smith C, Tam F, Tanna A, Tansey K, Tomlinson J, Webster P.

We also acknowledge the efforts of renal specialist doctors in training for assistance with recruiting patients to this study.

We acknowledge the Imperial College Research Computing Service (DOI: 10.14469/hpc/2232).

## Funding statement

This research was partly funded by Community Jameel and the Imperial President's Excellence Fund and by a UKRI-DHSC COVID-19 Rapid Response Rolling Call (MR/V027638/1) (to JEP), and by funding from UKRI/NIHR through the UK Coronavirus Immunology Consortium (UK-CIC) (to MB). We also acknowledge the National Institute for Health Research (NIHR) Biomedical Research Centre based at Imperial College Healthcare NHS Trust and Imperial College London. The views expressed are those of the author(s) and not necessarily those of the NHS, the NIHR or the Department of Health. JEP was supported by UKRI Innovation Fellowship at Health Data Research UK (MR/S004068/2). DCT is supported by a Stage 2 Wellcome-Beit Prize Clinical Research Career Development Fellowship (20661206617/A/17/Z and 206617/A/17/A) and the Sidharth Burman endowment. MCP is a Wellcome Trust Senior Fellow in Clinical Science (212252/Z/18/Z). NM-T and ES are supported by Wellcome Trust and Imperial College London Research Fellowships, and CLC by an Auchi Clinical Research Fellowship.

The funders had no role in study design, data collection and interpretation, or the decision to submit the work for publication.

## Competing interests

None of the authors have any patents (planned, pending or issued) or competing interests relevant to this work. Other interests unrelated to this work: SPM reports personal fees from Celltrion, Rigel, GSK and Cello; MCP reports consulting honoraria with Alexion, Apellis, Achillion, Novartis and Gyroscope; DCT reports speaker and consultancy fees from Astra-Zeneca and Novartis; JEP has received travel and accommodation expenses and hospitality from Olink to speak at Olink-sponsored academic meetings (none within the past 5 years). None of the other authors have any interests to declare.

## FIGURES



**Figure 1: Study design and cohort summary. A)** Graphical summary of the patient cohorts, sampling, and major analyses. **B/C)** For each cohort, the timing of the serial blood sampling is shown by triangles and the temporal COVID-19 severity by coloured bars. Three patients were hospitalised prior to COVID-19 diagnosis in the Wave 1 cohort. Three of the four patients in the Wave 2 cohort with fatal outcomes died >30 days from first positive swab.

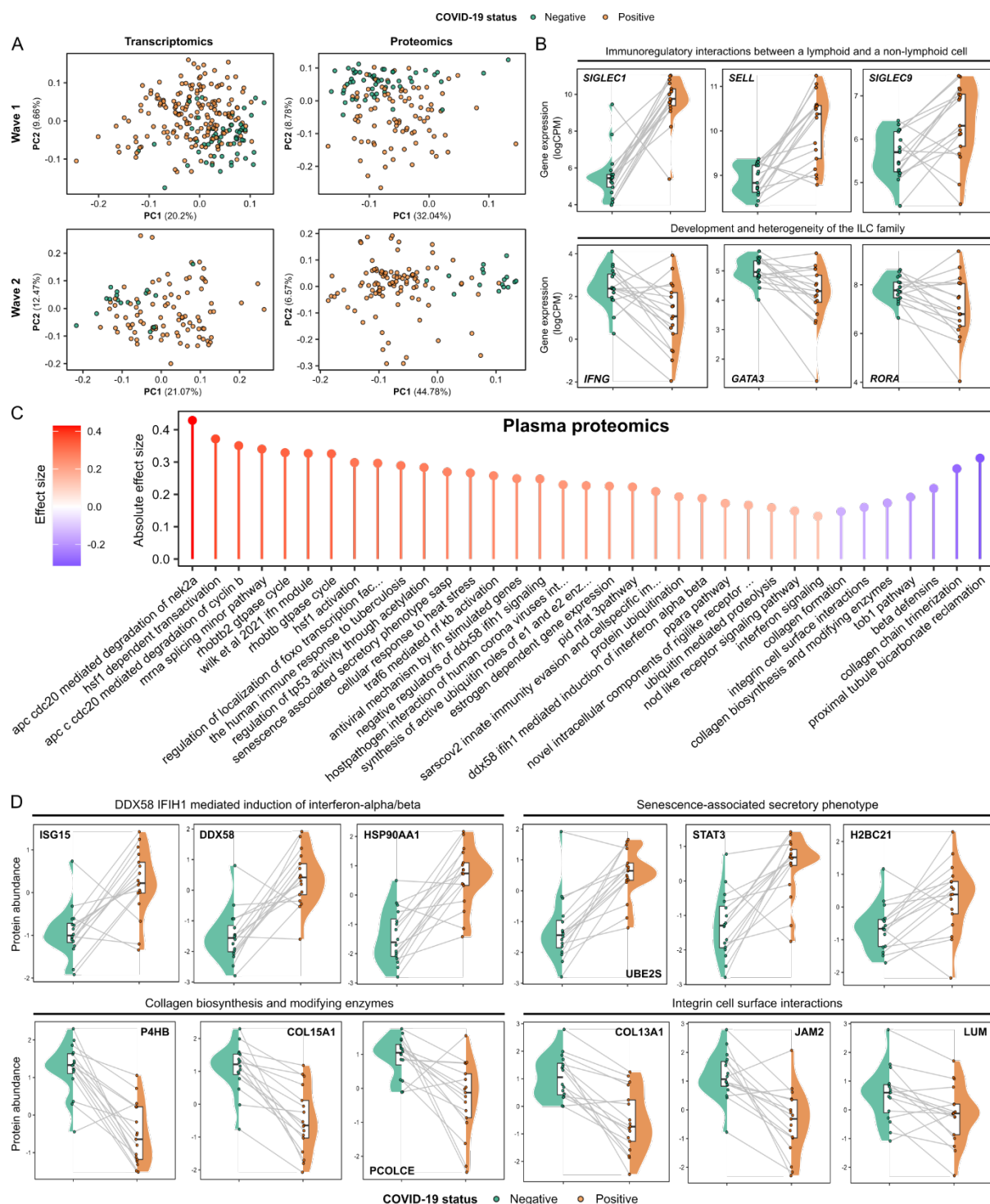


**Figure 2: Signatures of COVID-19 in ESKD.** **A)** PCA of the PBMC transcriptome (left) and plasma proteome (right). Each point represents a sample and is coloured by COVID-19 status. **B)** Paired violin plots showing intra-individual comparisons of pre-infection and most severe sample (Wave 2 cohort) during COVID-19 for selected genes. Grey lines link each individual's pre-infection and infection samples. All genes shown were significantly differentially expressed (1% FDR) in both cohorts. Genes are grouped by membership to pathways that were significantly enriched (1% FDR) in GSEA. **C)** The 30 protein pathway enrichment terms with the greatest RRA scores (indicating consistent dysregulation in both the Wave 1 and Wave 2 proteomic datasets), ordered by effect size. All pathway terms shown were significantly enriched in the individual cohort analyses (1% FDR). Red= up-regulated in COVID-19 versus controls; blue= down-regulated. **D)** As for **B**, but displaying selected plasma proteins (significant at 1% FDR).

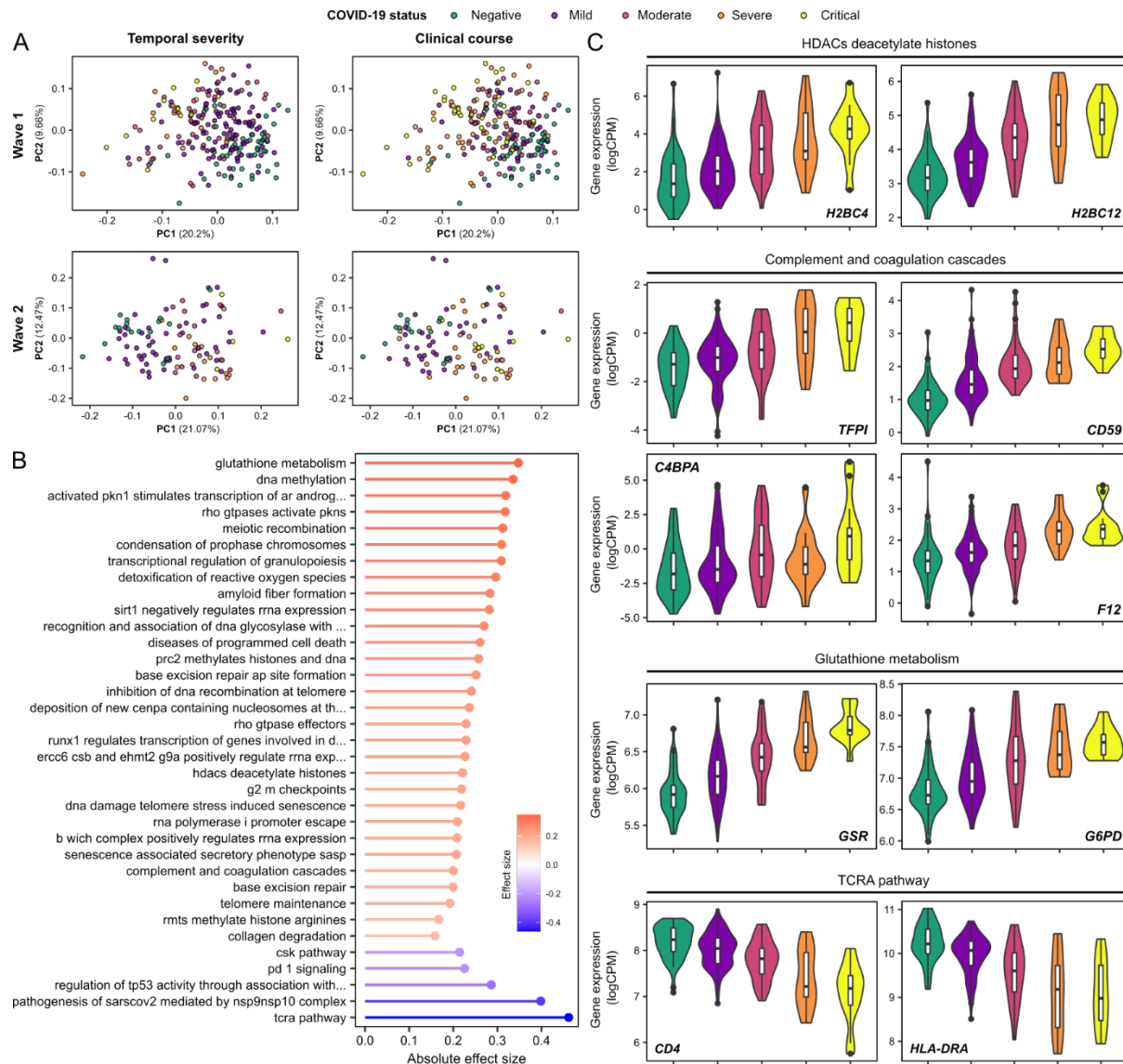


**Figure 3: Association of the PBMC transcriptome and COVID-19 severity.** **A)** PCA of the PBMC transcriptome. Each point represents a sample and is coloured by contemporaneous COVID-19 WHO severity (left) and overall clinical course (right). **B)** The 30 GSEA transcriptomic pathway enrichment terms with the greatest RRA scores. All were significantly enriched in both Wave 1 and 2 cohorts (1% FDR). Terms are ordered and coloured by their effect size. Red= up-regulated in more severe COVID-19; blue= down-regulated. **C)** Violin plots show gene expression values (Wave 1 cohort) stratified by COVID-19 status and severity (at time of sample) for selected genes. All genes shown were significantly associated (1% FDR) with severity in both the Wave 1 and 2 cohorts. Genes are grouped by membership to pathways that were significantly enriched (1% FDR) in GSEA.

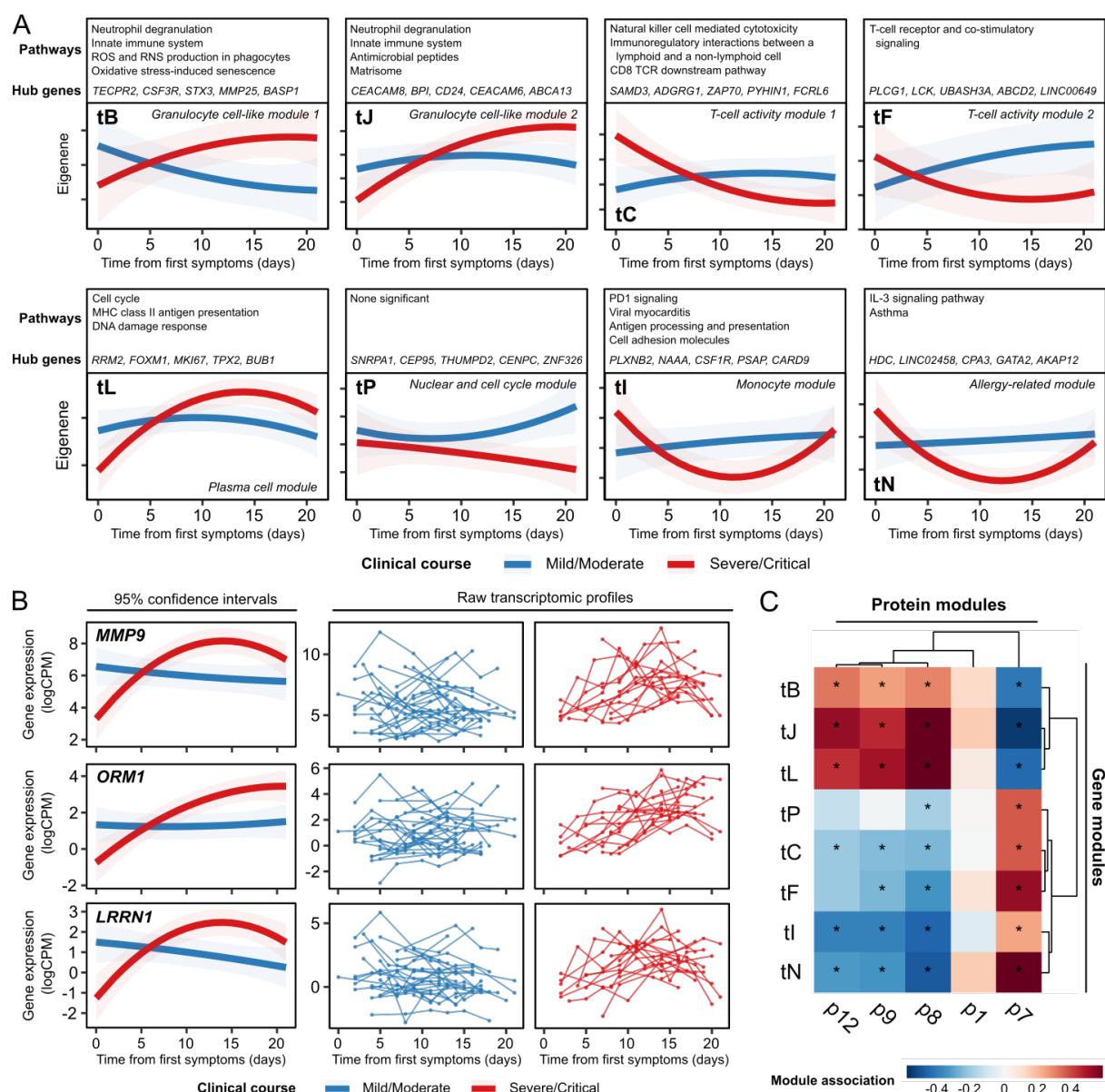


**Figure 4: Longitudinal profiles of transcriptomic modules.** **A)** The longitudinal profiles of significant (5% FDR) gene modules, stratified by clinical course. Lines represent model estimates and shaded areas represent 95% confidence intervals. **B)** Modelled longitudinal profiles of genes within module B with the most significant TxCC interaction effects. Left: model estimates and 95% confidence intervals. Right: individual-level data. **C)** Heatmap displaying associations (LMM) between transcriptomic and proteomic modules (right). Red= positive correlation, blue= negative correlation. Significant associations (5% FDR) are represented by an asterisk.

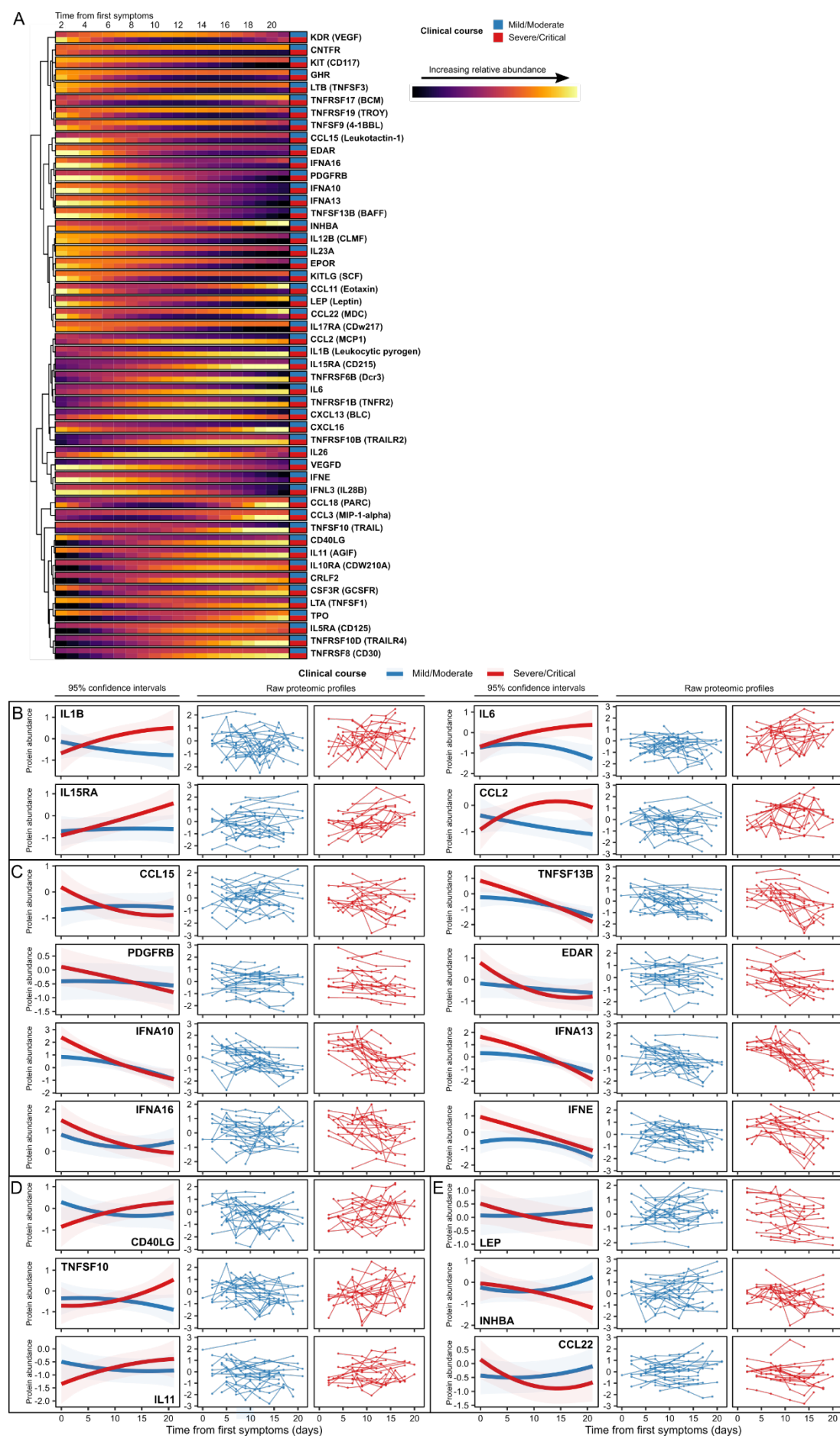


**Figure 5: Dynamic temporal changes in circulating cytokines and receptors vary between severe and mild COVID-19. A)** Heatmap displaying proteins with a significantly different temporal profile in mild vs severe disease (TxCC, LMM, FDR <0.05). Colour indicates model estimates over time, stratified by patient group. Proteins are clustered based on the temporal profile of the discordance between mild/moderate and severe/critical disease. Proteins are annotated using gene symbols, with alternative common protein identifiers in parentheses. **B-E)** Examples of proteins with differing patterns of discordance over time in severe/critical versus mild/moderate patients.

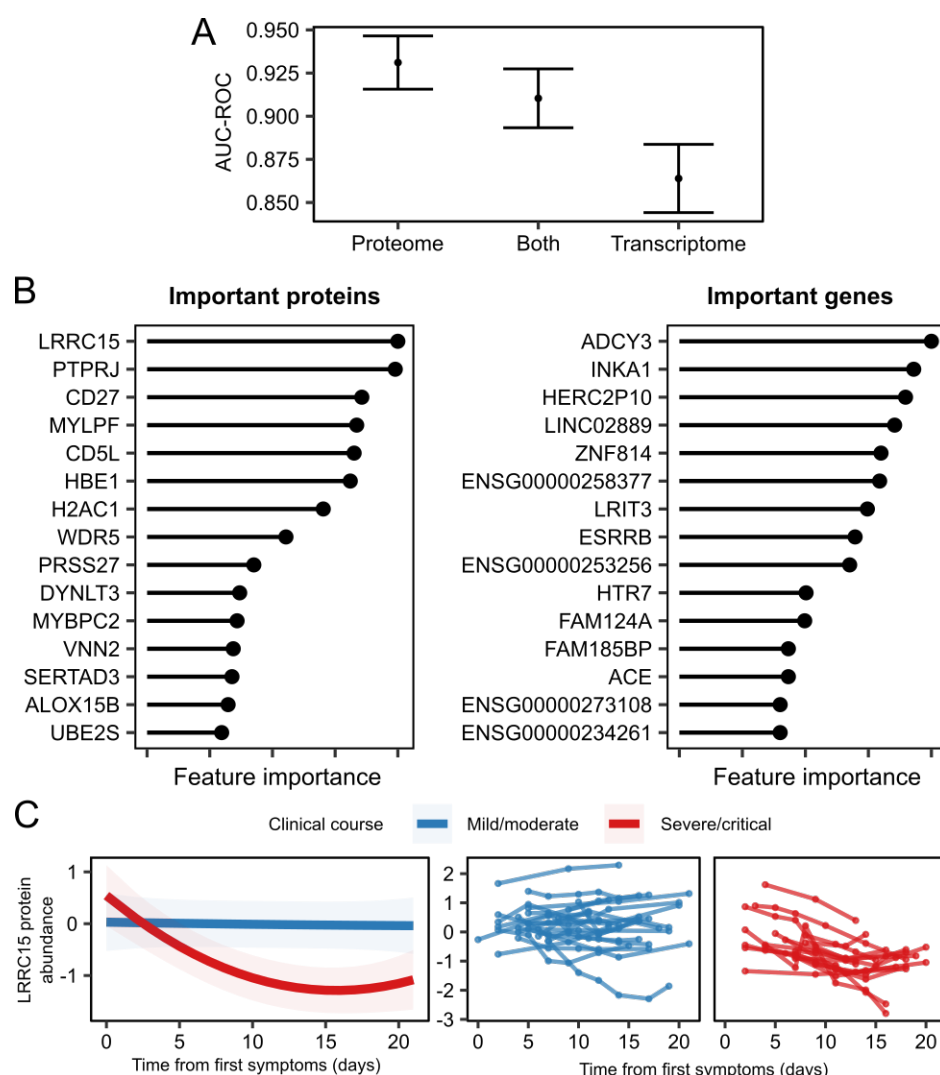


**Figure 6: Supervised learning to predict COVID-19 severity from molecular features. A)** Point estimates of area under the curve from receiver operator analysis (AUC-ROC) for predicting COVID-19 severity with 95% confidence intervals using lasso. “Both” = supervised learning on the combined proteomic and transcriptomic data. **B)** Important proteins (left) and genes (right) for the lasso model. Feature importance is scaled between 0 and 1, where 1 represents the most important feature. **C)** The profile of LRRC15 plasma protein concentration over time, stratified by severity of the patients’ overall clinical course. Left: model estimates and 95% confidence intervals ( $p < 0.0001$ , TxCC interaction, LMM). Right: raw data for each individual (right).

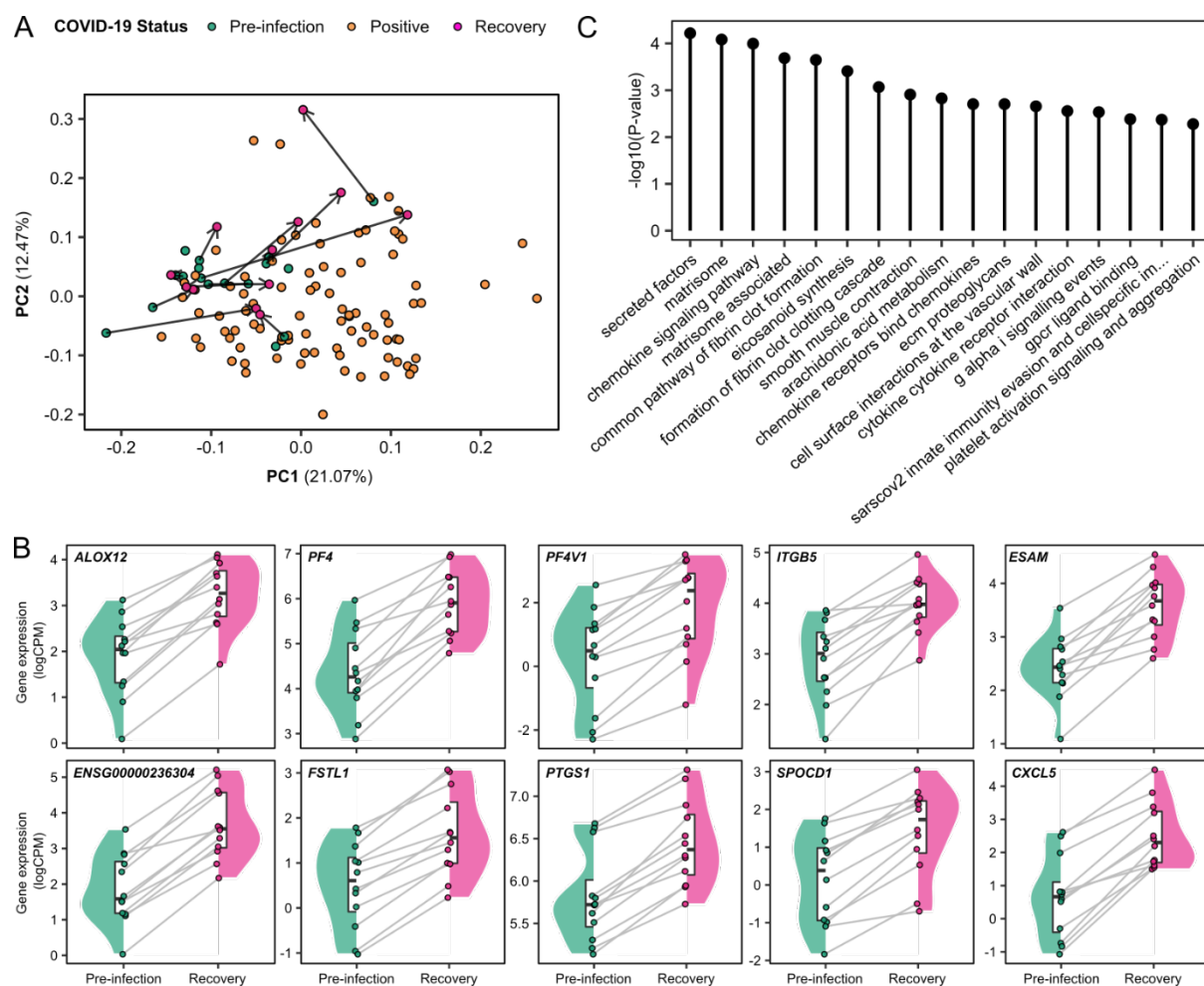


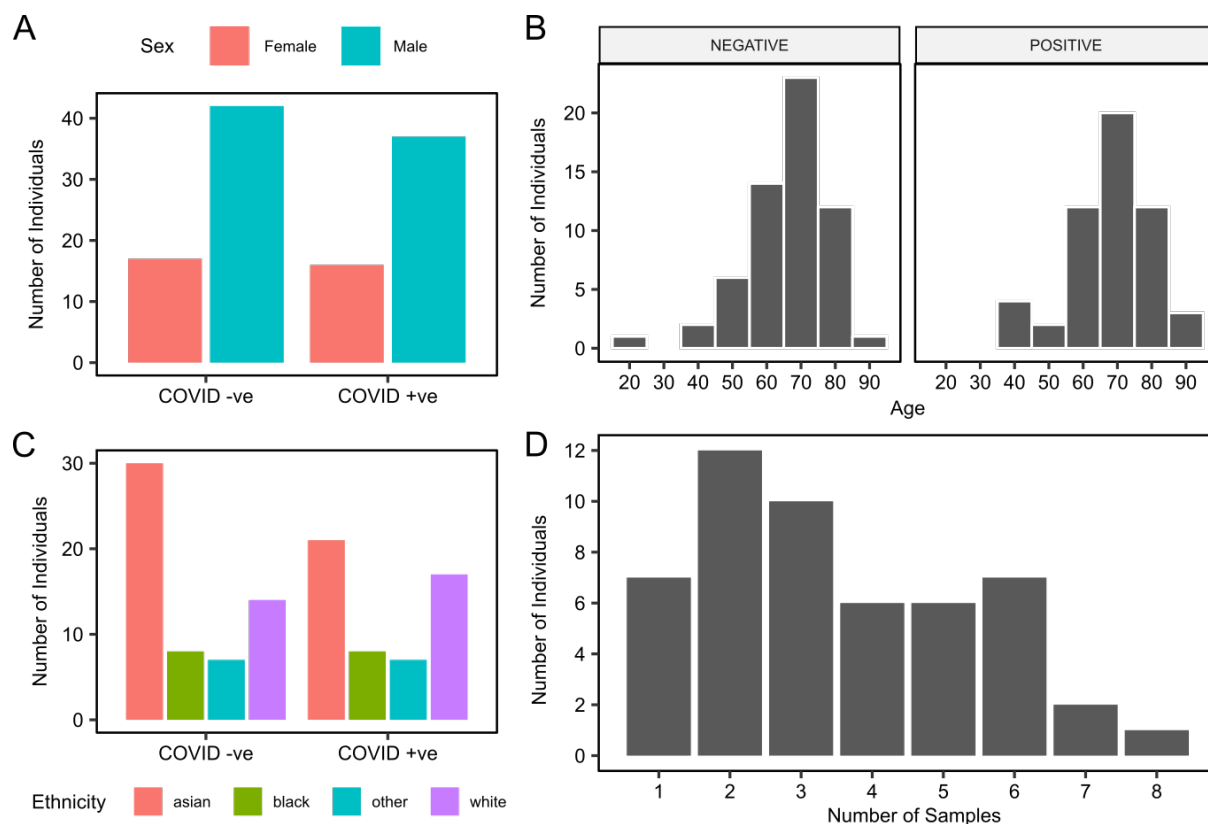
**Figure 7: Persistent dysregulation of immune cell gene expression two months following COVID-19.** **A)** PCA of the Wave 2 PBMC transcriptomic data, including pre-infection, infection and recovery samples (taken 2 months after the acute illness). Each point represents a sample. Arrows link recovery samples to the pre-infection sample from the same individual. **B)** Paired violin plots for differentially expressed genes in recovery versus pre-infection samples. Grey lines link each individual's pre-infection sample to their recovery sample. **C)** All significantly enriched (5% FDR) pathway terms for the differentially expressed genes in recovery versus pre-infection samples.

## TABLES

**Table 1: Genes that do not return to baseline 2 months after recovery from COVID-19.** Genes that are significantly differentially expressed (1% FDR) in recovery versus pre-infection samples. Estimate represents the average difference in log CPM (counts per million). A complete table including all genes tested can be found in **Supplementary Table recovery\_results**.

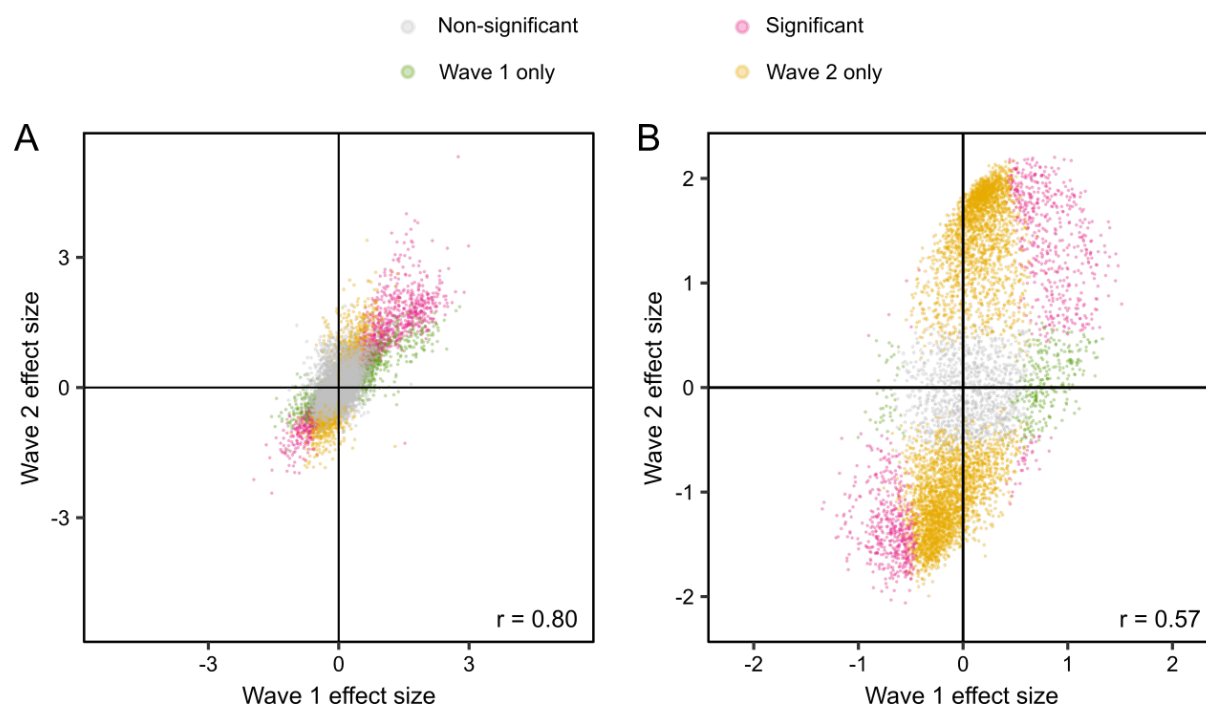
Gene ID	Gene name	Estimate (recovery - pre-infection)	P-value	Adjusted P-value
<i>ENSG00000236304</i>	lncRNA	1.84	5.37E-08	9.20E-04
<i>FSTL1</i>	Follistatin Like 1	1.17	1.60E-07	1.37E-03
<i>PTGS1</i>	Prostaglandin-Endoperoxide Synthase 1	0.64	3.69E-07	2.11E-03
<i>SPOCD1</i>	SPOC Domain Containing 1	1.31	6.41E-07	2.53E-03
<i>CXCL5</i>	C-X-C Motif Chemokine Ligand 5	1.84	7.39E-07	2.53E-03
<i>ALOX12</i>	Arachidonate 12-Lipoxygenase, 12S Type	1.33	1.24E-06	3.53E-03
<i>PF4</i>	Platelet Factor 4	1.53	1.71E-06	3.91E-03
<i>ESAM</i>	Endothelial Cell Adhesion Molecule	1.18	1.83E-06	3.91E-03
<i>MT-RNR1</i>	Mitochondrially Encoded 12S rRNA	1.00	2.61E-06	4.13E-03
<i>MMD</i>	Monocyte To Macrophage Differentiation Associated	0.77	2.80E-06	4.13E-03
<i>ENSG00000240093</i>	lncRNA	-0.71	2.82E-06	4.13E-03
<i>MTURN</i>	Maturin, Neural Progenitor Differentiation Regulator Homolog	0.54	3.11E-06	4.13E-03
<i>GNG11</i>	G Protein Subunit Gamma 11	1.53	3.13E-06	4.13E-03
<i>CAVIN2</i>	Caveolae Associated Protein 2	1.15	4.51E-06	5.52E-03
<i>DOK6</i>	Docking Protein 6	1.59	5.00E-06	5.71E-03
<i>LINC00989</i>	lncRNA	1.25	5.76E-06	5.81E-03
<i>SPARC</i>	Secreted Protein Acidic And Cysteine Rich	1.65	6.07E-06	5.81E-03
<i>PF4V1</i>	Platelet Factor 4 Variant 1	1.60	6.11E-06	5.81E-03
<i>ABLIM3</i>	Actin Binding LIM Protein Family Member 3	1.41	6.88E-06	6.07E-03
<i>MFAP3L</i>	Microfibril Associated Protein 3 Like	0.74	7.09E-06	6.07E-03
<i>CALD1</i>	Caldesmon 1	1.78	7.79E-06	6.23E-03
<i>ITGB5</i>	Integrin Subunit Beta 5	1.10	8.00E-06	6.23E-03
<i>LINC01750</i>	lncRNA	2.00	1.13E-05	8.22E-03
<i>PCSK6</i>	Proprotein Convertase Subtilisin/Kexin Type 6	1.22	1.15E-05	8.22E-03
<i>PVALB</i>	Parvalbumin	2.04	1.46E-05	9.97E-03

## Supplementary Figures



**Supplementary Figure 1: Characteristics of the Wave 1 cohort.** The number of COVID-19 positive and negative patients, stratified by **A**), sex **B**), age **C**) ethnicity. **D**) Number of serial PBMC samples with post-QC RNA-seq data available for COVID-19 patients.

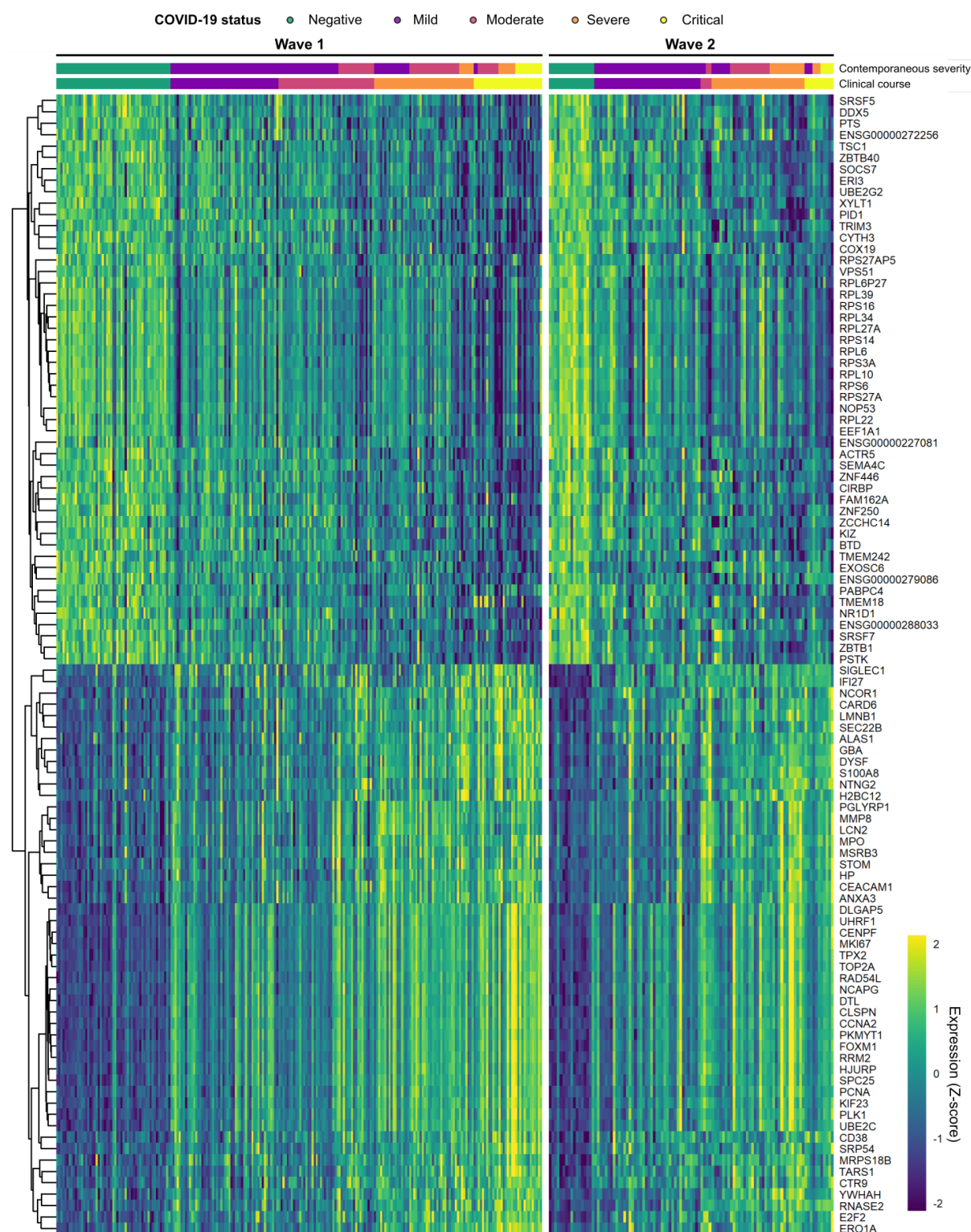
1147



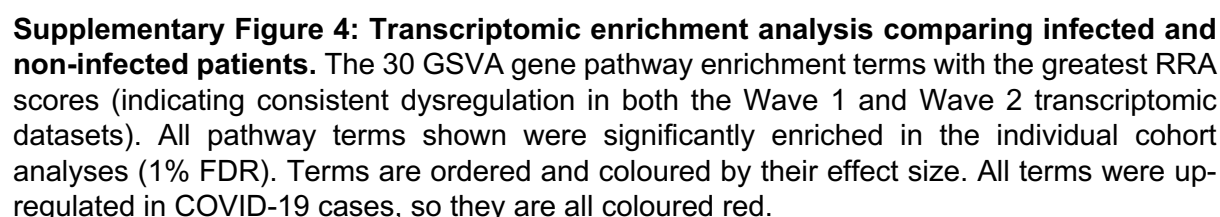
1148

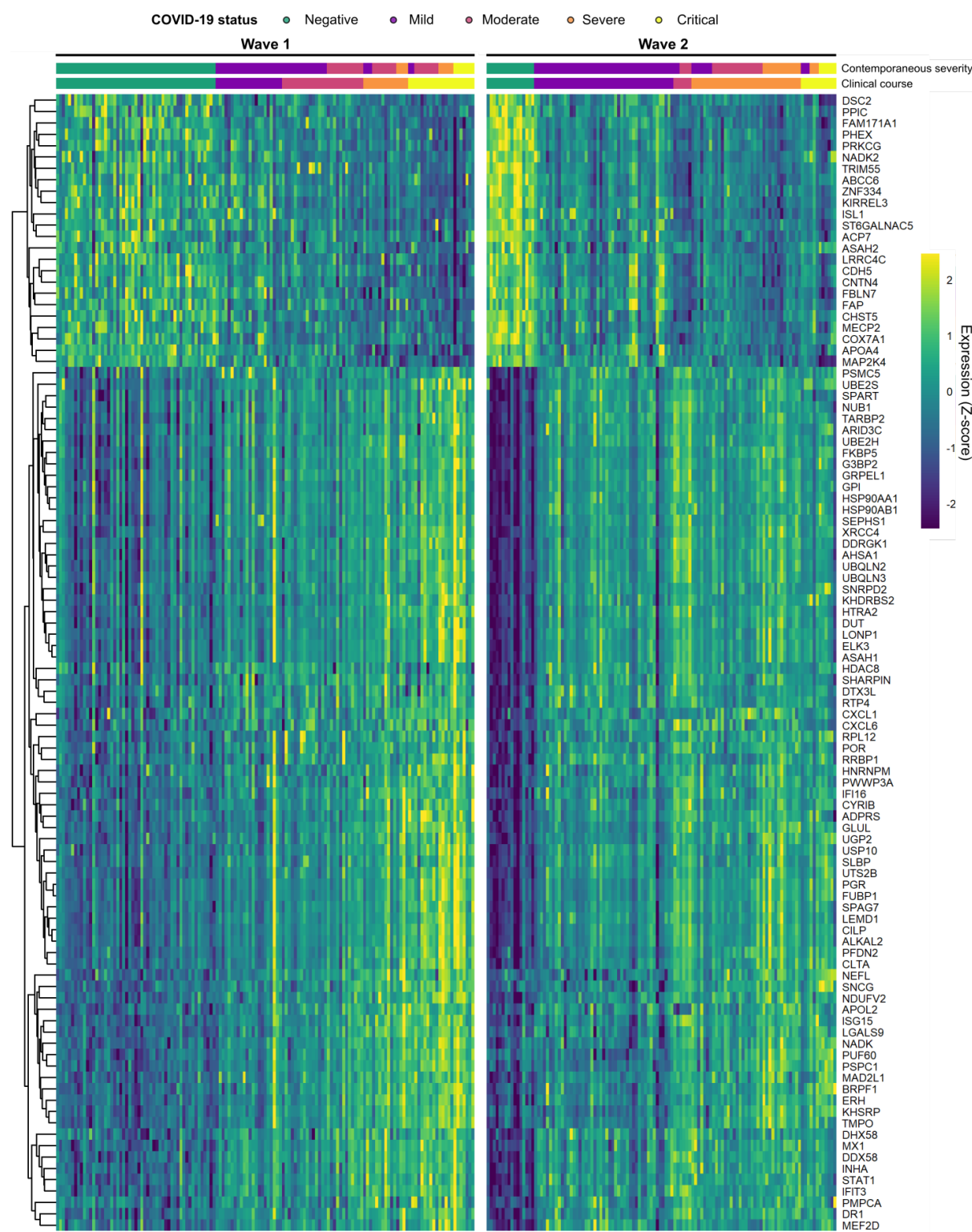
1149

1150 **Supplementary Figure 2: A)** Comparison of effect sizes (coefficients from LMM) for the Wave  
1151 1 and Wave 2 infected vs non-infected differential expression analyses for the transcriptome.  
1152 Each point is a gene, coloured according to its significance in the Wave 1 and 2 analyses.  $r =$   
1153 Pearson's correlation coefficient. **B)** As A, for the proteome.



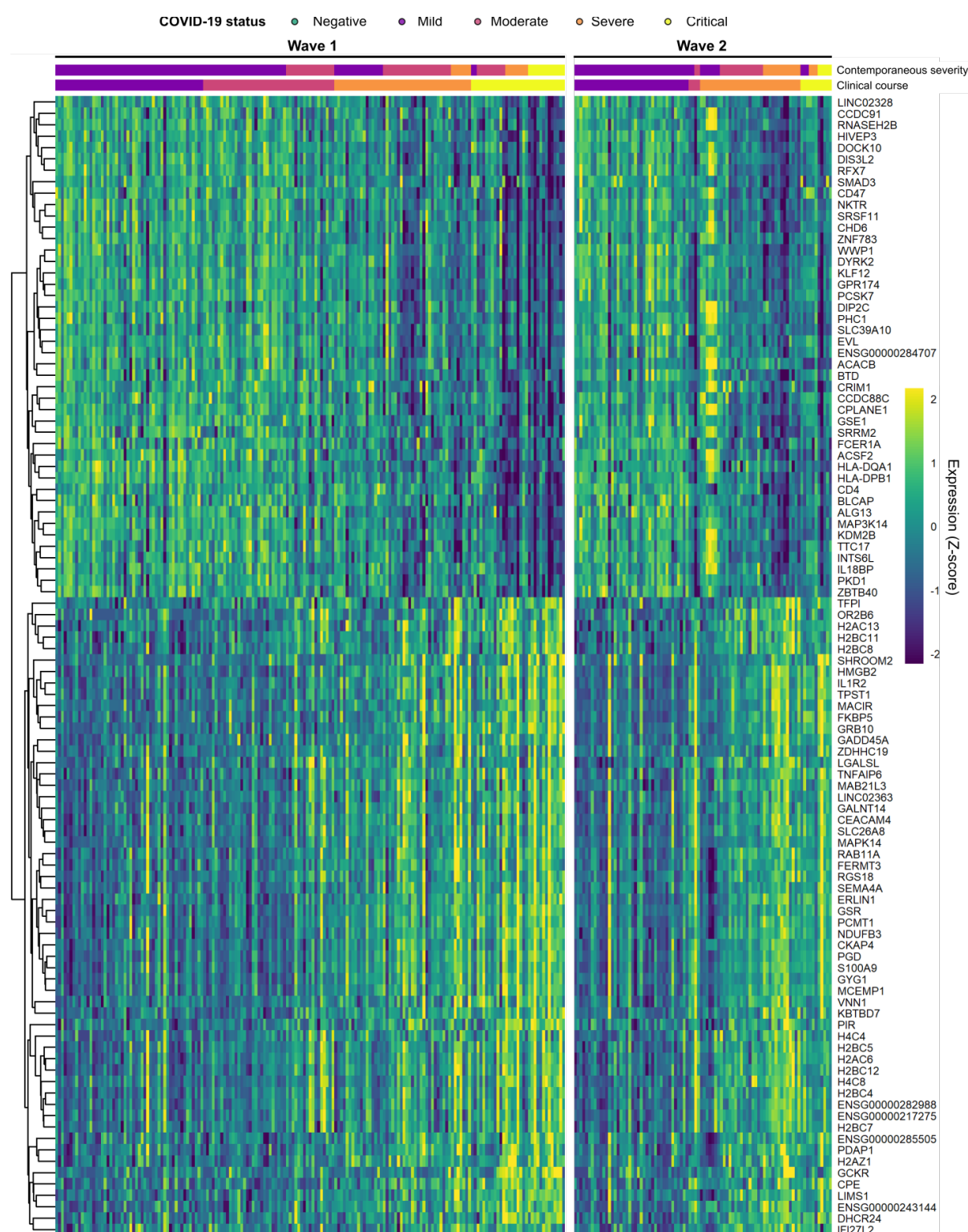
**Supplementary Figure 3: Genes differentially expressed in COVID-19.** Heatmap for the 100 transcriptomic features most significantly differentially expressed between COVID-19 cases and controls, according to robust rank aggregation (RRA). These genes were significant in both cohorts (1% FDR). Columns are ordered by COVID-19 status and severity. For the Wave 1 heatmap, genes are ordered by hierarchical clustering; the Wave 2 heatmap is ordered to match this. Each feature was scaled and centred separately in each dataset.





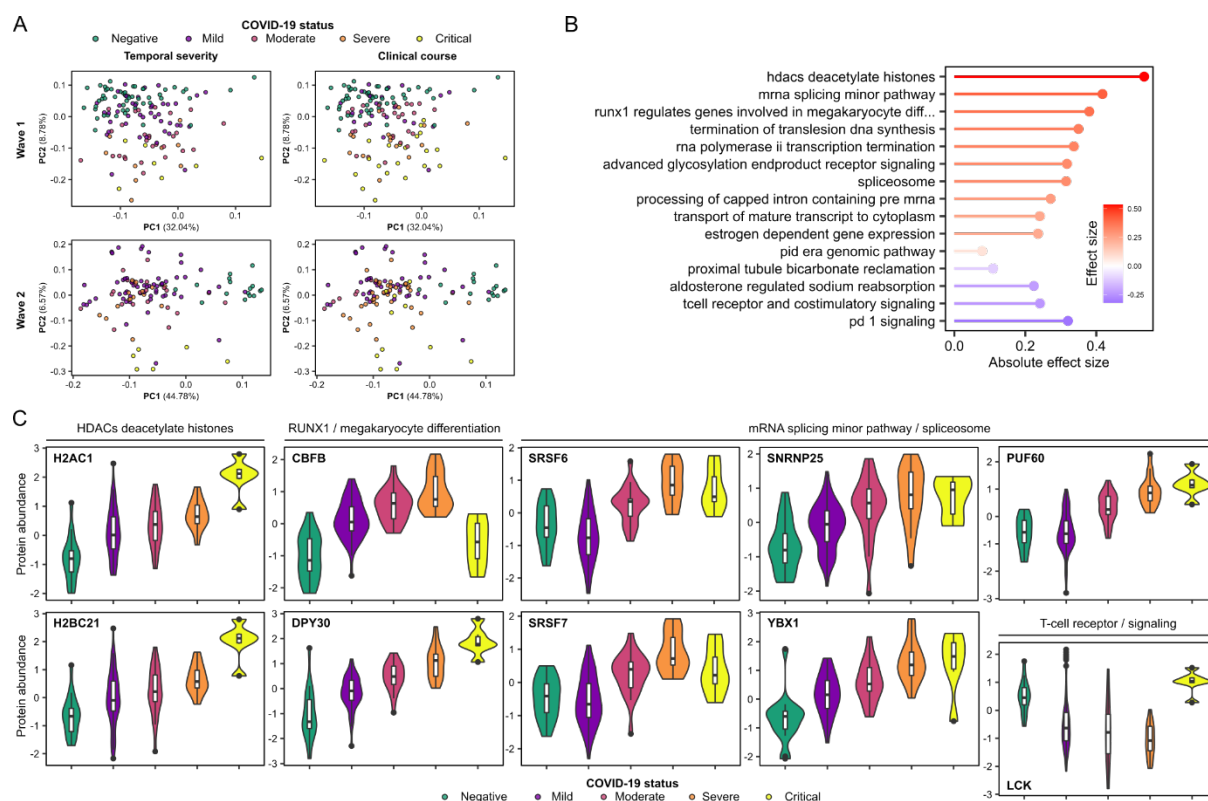
**Supplementary Figure 5: Most significant differentially abundant plasma proteins in COVID-19 positive versus negative ESKD samples.** Heatmap for the 100 proteomic features most significantly differentially abundant between COVID-19 cases and controls, according to robust rank aggregation (RRA). These proteins were significant in both cohorts (1% FDR, LMM). Columns are ordered by COVID-19 status and severity. For the Wave 1 heatmap, proteins are ordered by hierarchical clustering; the Wave 2 heatmap is ordered to match this. Each feature was scaled and centred separately in each dataset.

1179

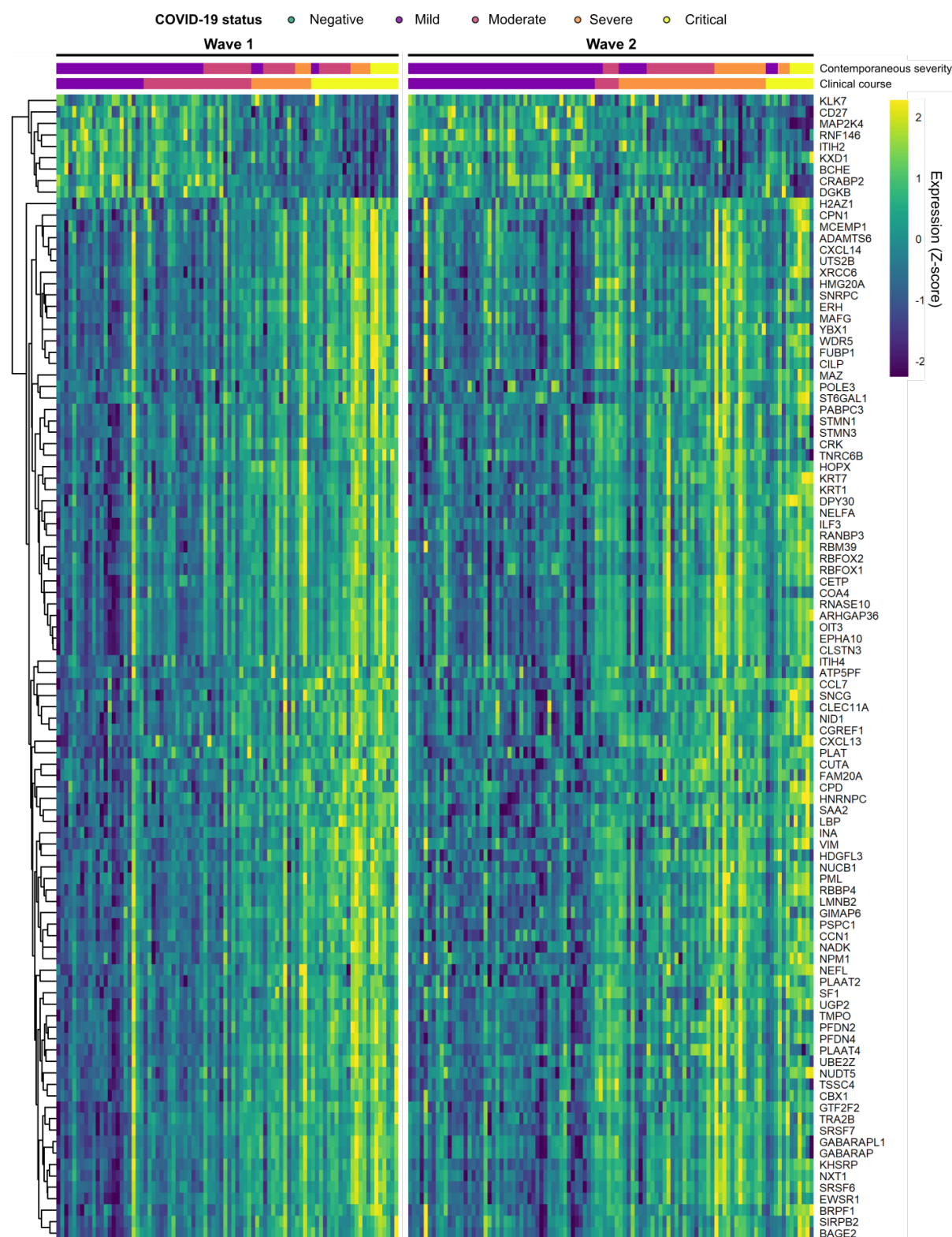


1180

1181 **Supplementary Figure 6: Genes with the most significant association with COVID-19**  
1182 **severity.** Heatmap for the 100 transcriptomic features most significantly associated with  
1183 contemporaneous severity, according to robust rank aggregation (RRA). These genes were  
1184 significant in both cohorts (1% FDR). Columns are ordered by COVID-19 status and severity.  
1185 For the Wave 1 heatmap, genes are ordered by hierarchical clustering; the Wave 2 heatmap  
1186 is ordered to match this. Each feature was scaled and centred separately in each dataset.

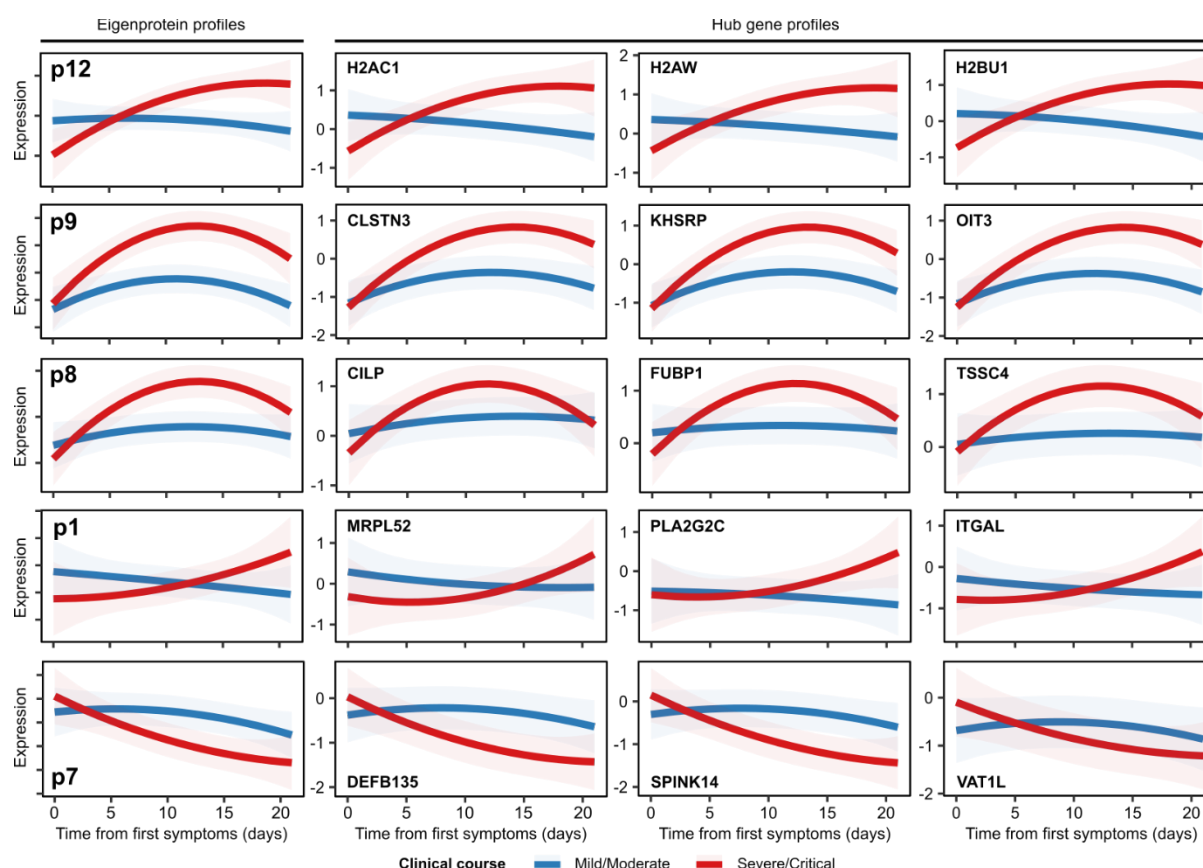


**Supplementary Figure 7: Plasma proteomic associations with COVID-19 severity. A)** PCA of the proteome. Each point represents a sample and is coloured by contemporaneous COVID-19 severity (left) and overall clinical course of the patient (right). **B)** The GSEA protein pathway enrichment terms significantly associated (1% FDR) with contemporaneous severity in both the Wave 1 and Wave 2 proteomic datasets. All pathway terms shown were significantly enriched in the individual cohort analyses (1% FDR). Terms are ordered and coloured by their effect size. Terms up-regulated in more severe COVID-19 are coloured red while down-regulated terms are blue. **C)** Violin plots show gene expression values (Wave 2 cohort) stratified by COVID-19 status and severity (at time of sample) for selected genes. All genes shown were significantly associated (1% FDR) with contemporaneous severity in the Wave 2 cohort.



**Supplementary Figure 8: Selected proteins associated with COVID-19 severity.** Heatmap for the 100 proteomic features most significantly associated with contemporaneous WHO severity, according to robust rank aggregation (RRA). These proteins were significant in both cohorts (1% FDR). Columns are ordered by COVID-19 status and severity. For the Wave 1 heatmap, proteins are ordered by hierarchical clustering; the Wave 2 heatmap is ordered to match this. Each feature was scaled and centred separately in each dataset.

1209



1210

1211

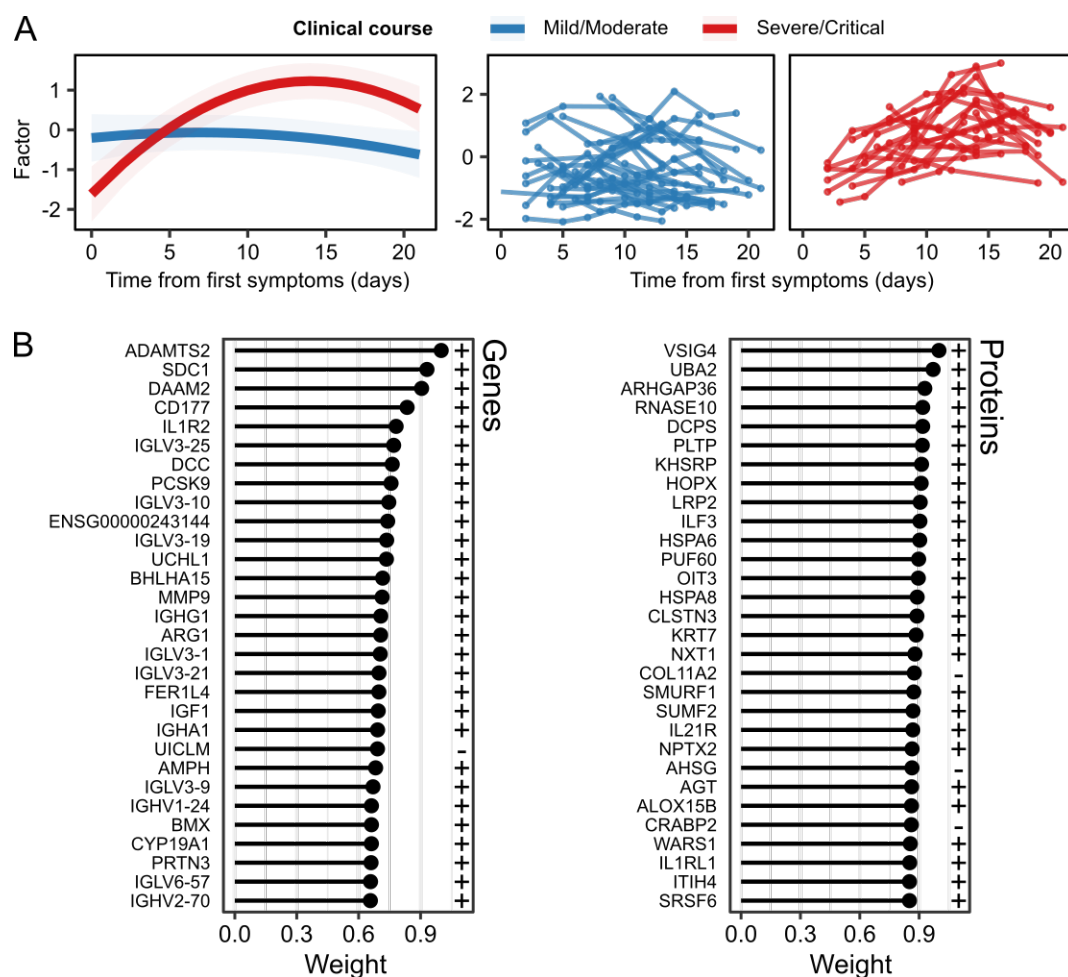
1212 **Supplementary Figure 9: Longitudinal profiles of protein modules and hub proteins.**

1213 Modelled longitudinal profiles of protein modules with significant (5% FDR) TxCC interactions

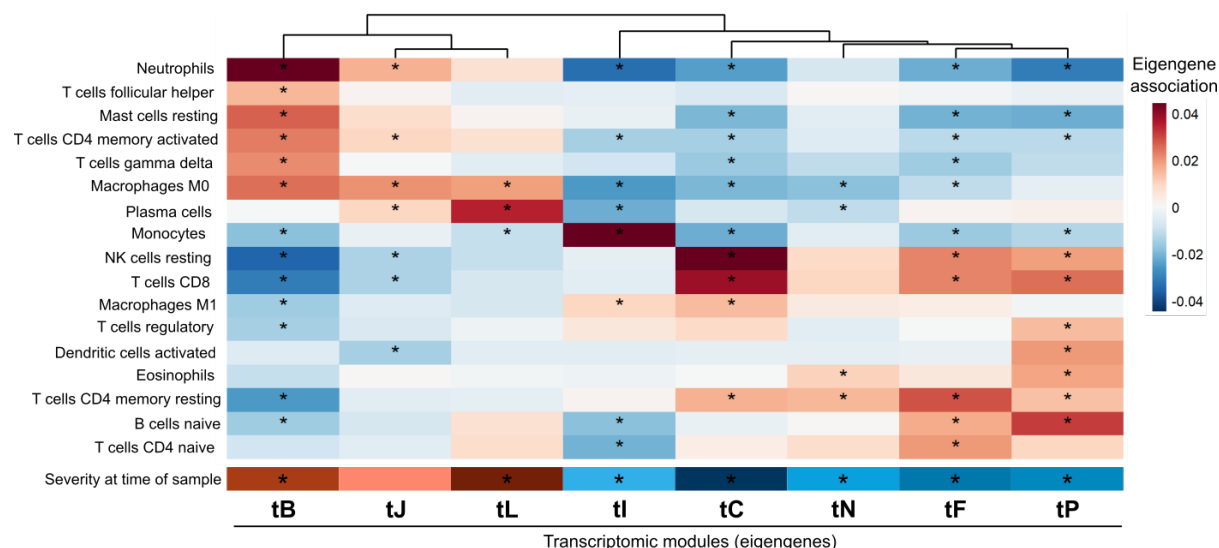
1214 (left) and the profiles of their top three most central hub proteins (right). Red lines= patients

1215 with a severe/critical clinical course; blue lines= mild/moderate clinical course. Shaded areas

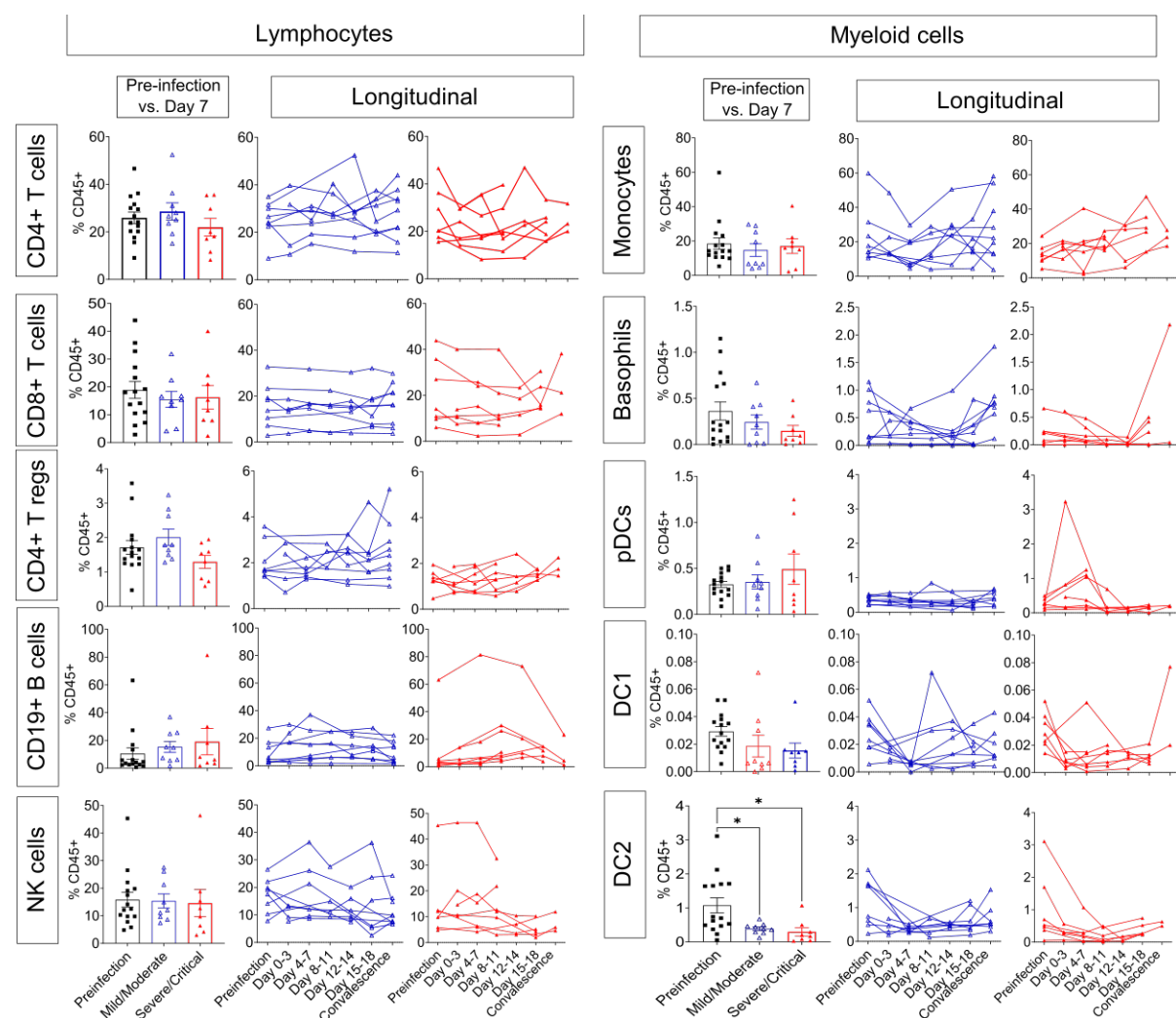
represent 95% confidence intervals.



**Supplementary Figure 10: A multi-modal factor representing COVID-19 severity. A)** The longitudinal profile of a factor identified by MEFISTO with a significant (5% FDR) TxCC interaction. Model estimates and 95% confidence interval (left) and the trajectory of the factor for each individual (right). **B)** The weights of individual genes and proteins with respect to the factor identified by MEFISTO. A plus sign indicates molecules positively associated with the factor while molecules negatively associated with the factor have a minus sign.



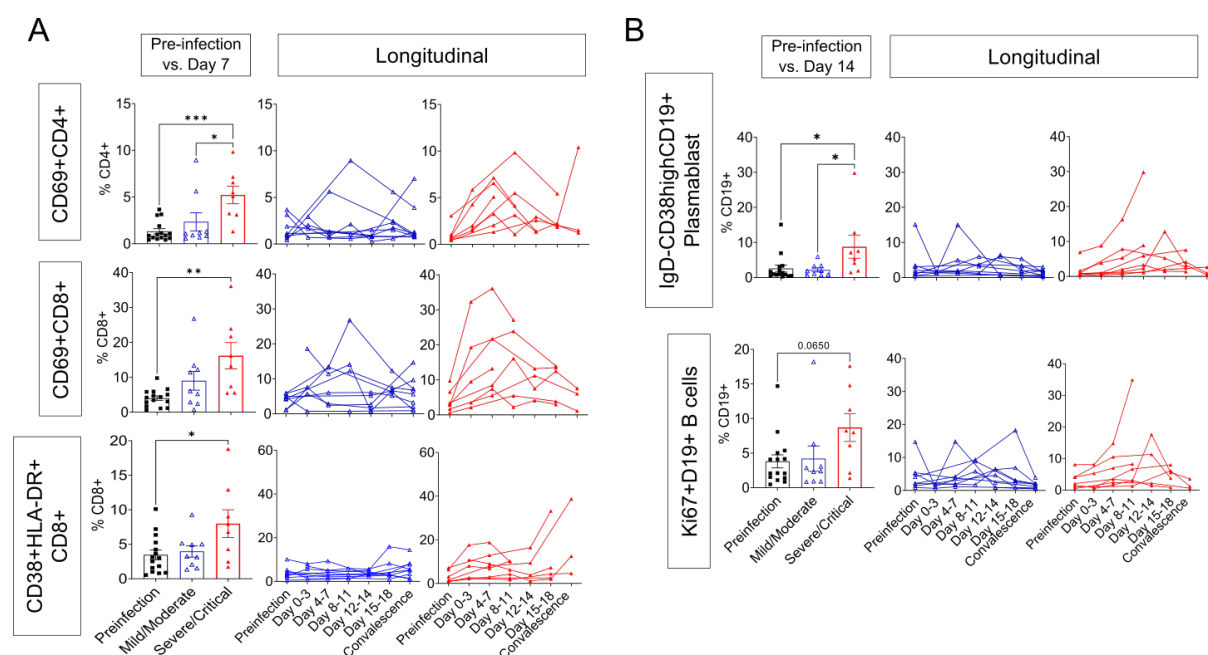
**Supplementary Figure 11: Association of transcriptomic modules with imputed cell abundances.** Association of modules (columns) with cell abundances (rows) imputed using CIBERSORTx. Analysis with LMM. All modules shown have significant TxCC interaction effects. The bottom row shows the association with severity score at time of sample. Asterisks represent significant (5% FDR) associations.



**Supplementary Figure 12: Proportion of major lymphocytes and myeloid cells in PBMCs (Wave 2 cohort).**

Panels marked “Pre-infection vs. Day 7”: frequencies of major immune subsets gated on CD45+ leukocytes in samples taken prior to infection (Pre-infection n=15) and at closest sample to day 7 from symptom onset (Mild/moderate n=9; Severe/critical n=8). Data presented as mean (box) ± S.E.M (whiskers). Each symbol represents an individual.

Panels marked “Longitudinal”: frequencies of major immune subsets before, during and after infection as a line plot. Each line depicts one individual. Blue = patients with a mild/moderate clinical course; sample numbers: Pre-infection n=8, Day 0-3 n=4, Day 4-7 n=6, Day 8-11 n=4, Day 12-14 n=6, Day 15-18 n=5, Convalescence n=9. Red= severe/critical clinical course; sample numbers: Pre-infection n=7, Day 0-3 n=5, Day 4-7 n=6, Day 8-11 n=6, Day 12-14 n=4, Day 15-18 n=5, Convalescence n=3. One-way ANOVA with Dunnett’s for multiple comparisons correction was used for statistical analysis. Only significant differences are indicated. \*p <0.05. NK= natural killer; pDCs= plasmacytoid dendritic cells. DC= dendritic cells.

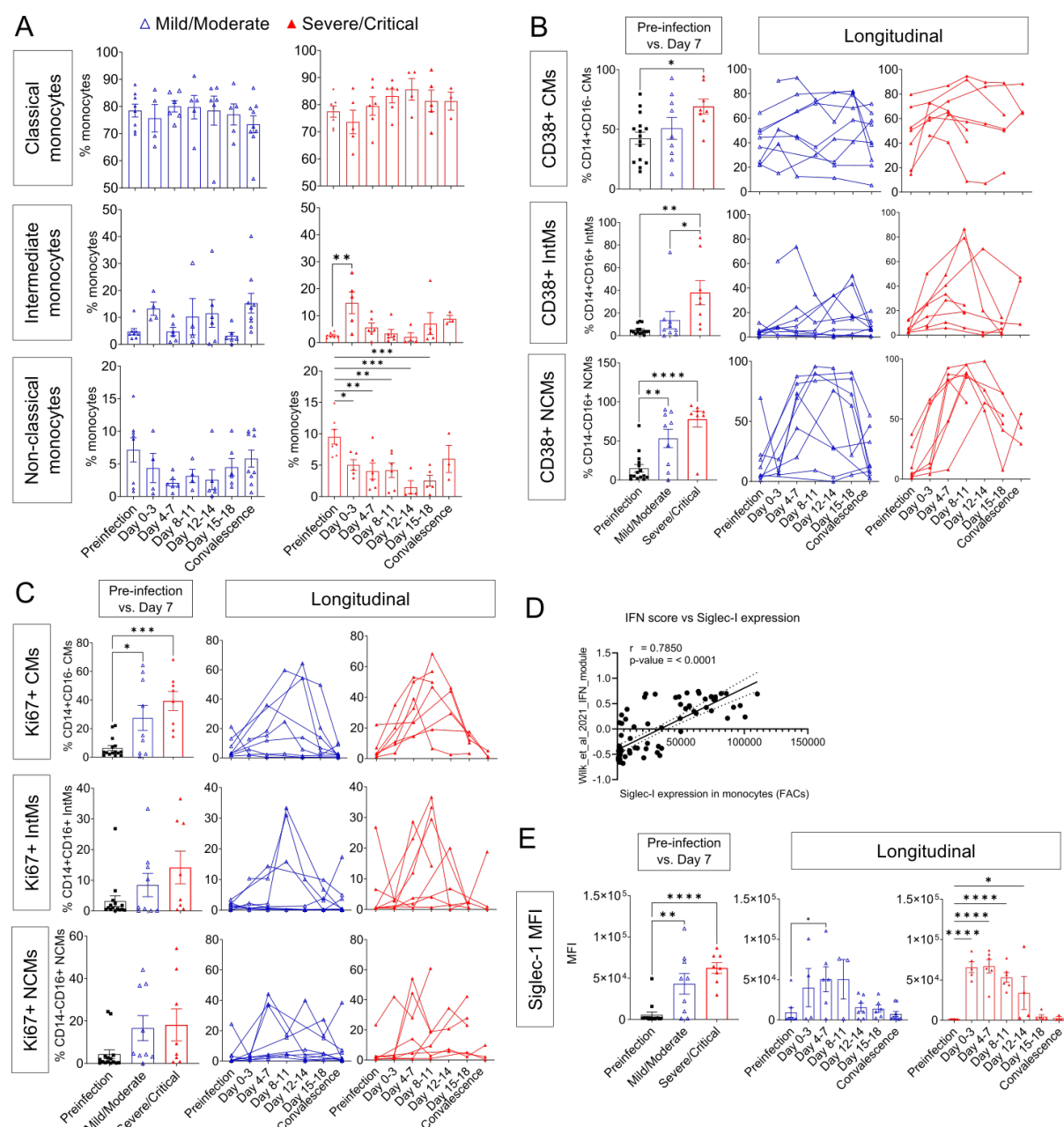


**Supplementary Figure 13: Increased activated T cells, plasmablast and proliferating B cells is associated with disease severity in COVID-19 ESKD patients.**

**A) Percentage of cells expressing activation markers CD69, CD38 and HLA-DR gated on CD4+ T cells or CD8+ T cells.** Panel marked “Pre-infection vs. Day 7”: data plotted for samples taken prior to infection (Pre-infection n=15) and for closest sample to day 7 from symptom onset (Mild/Moderate n=9; Severe/Critical n=8).

**B) Frequencies of IgD-CD38<sup>hi</sup>CD19+ plasmablast and Ki67+ cells gated on CD19+ B cells.** Panel marked “Pre-infection vs. Day 14”: data plotted for samples taken prior to infection (Pre-infection n=15) and for closest sample to day 14 from symptom onset (Mild/Moderate n=9; Severe/Critical n=8).

(A-B) Left panels: data presented as mean (bar) ± S.E.M (whiskers). Each symbol represents an individual. Right panels: frequencies of cells over the course of infection as a line plot. Each continuous line depicts one individual. Mild/moderate patients in blue (Pre-infection n=8, Day 0-3 n=4, Day 4-7 n=6, Day 8-11 n=4, Day 12-14 n=6, Day 15-18 n=5, Convalescence n=9) and severe/critical in red (Pre-infection n=7, Day 0-3 n=5, Day 4-7 n=6, Day 8-11 n=6, Day 12-14 n=4, Day 15-18 n=5, Convalescence n=3). One-way ANOVA with Dunnett’s for multiple comparisons correction used for statistical analysis. Only significant differences are indicated. \*p < 0.05; \*\*p < 0.01; \*\*\*p < 0.001.



**Supplementary Figure 14: Increased activated and proliferating circulatory monocytes is associated with disease severity in COVID-19 ESKD patients.**

**A)** Frequencies of monocyte subsets as defined with CD14+ and CD16+ expression gated on total monocytes. Percentage of cells expressing CD38 (**B**) and Ki67 (**C**) gated on CD14+CD16- CMs, CD14+CD16+ IntMs, CD14-CD16+ NCMs. **D)** Correlation (Pearson's  $r$ ) of SIGLEC-1 protein expression by MFI to RNAseq-derived GSVA enrichment score for type I IFN signatures. **E)** Siglec-1 expression in MFI gated on total monocytes.

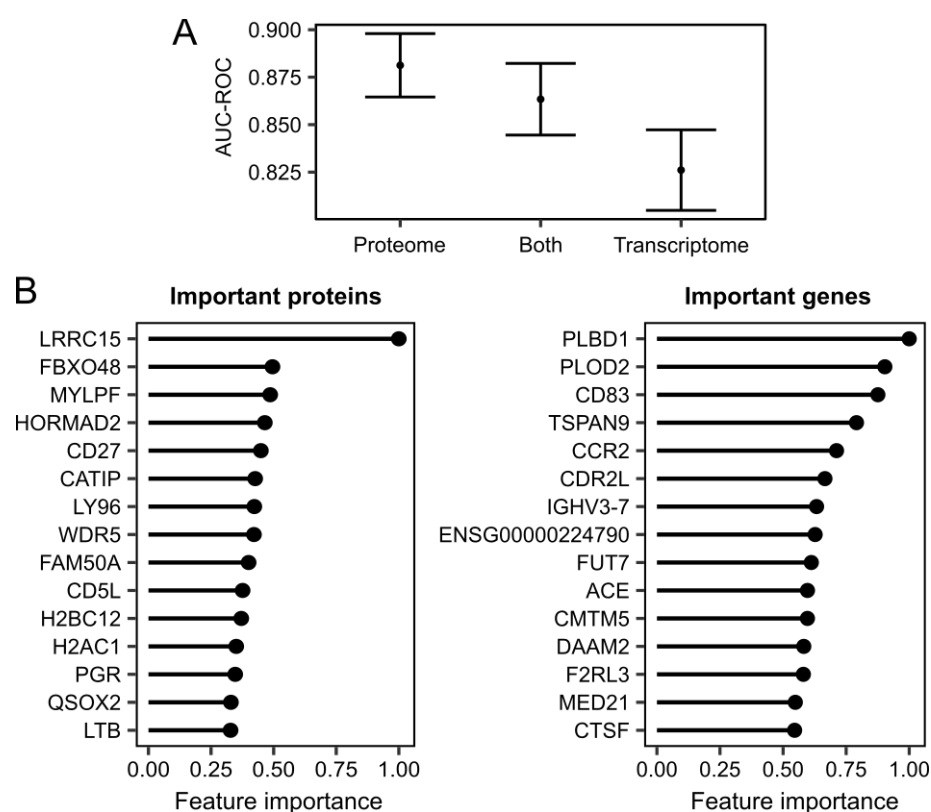
(B, C, E): Data plotted for samples taken prior to infection (Pre-infection  $n=15$ ) and for closest sample to day 7 from symptom onset (Mild/Moderate  $n=9$ ; Severe/Critical  $n=8$ ). Data presented as mean  $\pm$  S.E.M. Each symbol represents an individual. (A, B, C, E) Frequencies of cells over the course of infection as a line or bar plot. Mild/moderate patients in blue (Pre-infection  $n=8$ , Day 0-3  $n=4$ , Day 4-7  $n=6$ , Day 8-11  $n=4$ , Day 12-14  $n=6$ , Day 15-18  $n=5$ , Convalescence  $n=9$ ) and severe/critical in red (Pre-infection  $n=7$ , Day 0-3  $n=5$ , Day 4-7  $n=6$ , Day 8-11  $n=6$ , Day 12-14  $n=4$ , Day 15-18  $n=5$ , Convalescence  $n=3$ ).

1287 (A, B, C, E): One-way ANOVA with Dunnet's for multiple comparisons correction used for  
1288 statistical analysis.

1289 Only significant differences are indicated. \*p <0.05; \*\*p <0.01; \*\*\*p <0.001. CM=Classical  
1290 Monocytes; IntM=Intermediate Monocytes; NCM=Non-classical Monocytes; MFI=Median  
1291 Fluorescence Intensity.

1292

1293



1294

1295

1296

1297

1298

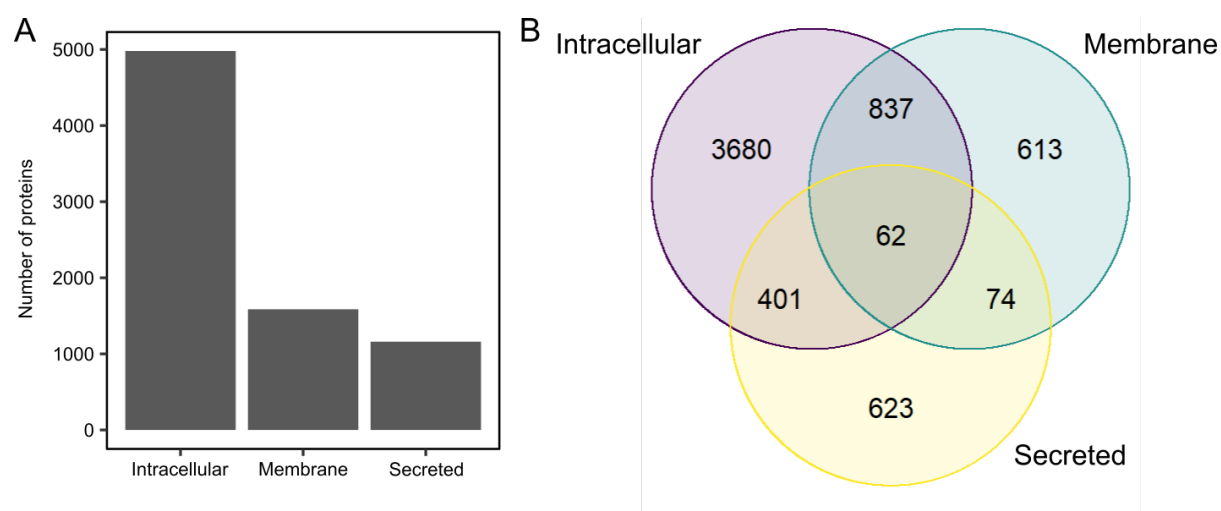
1299

1300

1301

1302

**Supplementary Figure 15: Predicting COVID-19 severity using random forests.** **A)** Point estimates of area under the curve from receiver operator analysis (AUC-ROC) for predicting COVID-19 severity with 95% confidence intervals using random forests. “Both” = supervised learning on the combined proteomic and transcriptomic data. **B)** Important proteins (left) and genes (right) for the random forests model. Feature importance is scaled between 0 and 1, where 1 represents the most important feature.



**Supplementary Figure 16: Human Protein Atlas classification of proteins measured by the SomaScan v4.1 assay.** A) The number of unique proteins measured that were labelled as intracellular, membrane and secreted. B) Venn diagram illustrating overlap between the annotations.

## Supplementary Tables

**Supplementary Table 1: Characteristics of the Wave 1 cohort.**

	Overall (n = 53)	Peak severity mild or moderate (n = 28)	Peak severity severe or critical (n = 25)
<b>Age</b>			
Median	72.0	73.0	68.0
(IQR)	62.0-76.0	64.8-76.2	62.0-76.0
<b>Sex</b>			
M	37 (69.8%)	18 (64.3%)	19 (76.0%)
F	16 (30.2%)	10 (35.7%)	6 (24.0%)
<b>Ethnicity</b>			
Asian	21 (39.6%)	11 (39.3%)	10 (40.0%)
White	17 (32.1%)	6 (21.4%)	11 (44.0%)
Black	8 (15.1%)	5 (17.9%)	3 (12.0%)
Other	7 (13.2%)	6 (21.4%)	1 (4.0%)
<b>Diabetes</b>	32* (60.4%)	16* (57.1%)	16 (64.0%)
<b>Current smoker</b>	1 (1.9%)	1 (3.6%)	0 (0.0%)
<b>ESKD cause</b>			
DN	27 (50.9%)	14 (50.0%)	13 (52.0%)
HTN/vascular	5 (9.4%)	3 (10.7%)	2 (8.0%)
GN/autoimmune	3 (5.7%)	1 (3.6%)	2 (8.0%)
Genetic	1 (1.9%)	1 (3.6%)	0 (0.0%)
Other/unknown	17 (32.1%)	9 (32.1%)	9 (36.0%)
<b>Hospitalisation due to COVID-19†</b>	32 (60.4%)	7 (25.0%)	25 (100%)
<b>Fatal COVID-19</b>	9 (17.0%)	0 (0.0%)	9 (36.0%)

DN = diabetic nephropathy. GN = glomerulonephritis. HTN = hypertension. IQR = inter-quartile range. Subsets defined according to peak WHO severity over the course of the illness.

\*One patient had type 1 diabetes, the remainder type 2. †3 patients were hospitalised prior to COVID-19 diagnosis. 8 patients diagnosed with COVID-19 as outpatients subsequently deteriorated were hospitalised.

**Supplementary Table 2: Characteristics of the Wave 2 cohort.**

	Overall (n = 17)	Peak severity mild or moderate (n = 9)	Peak severity severe or critical (n = 8)
<b>Age</b> Median (IQR)	72.0 61.0-77.0	72.0 60.0-75.0	70.5 64.0-80.5
<b>Sex</b> M F	10 (58.8%) 7 (41.2%)	4 (44.4%) 5 (55.6%)	6 (75.0%) 2 (25.0%)
<b>Ethnicity</b> Asian White Black Other	11 (64.7%) 4 (23.5%) 1 (5.9%) 1 (5.9%)	6 (66.7%) 2 (22.2%) 0 (0.0%) 1 (11.1%)	5 (62.5%) 2 (25.0%) 1 (12.5%) 0 (0.0%)
<b>Diabetes</b>	11 (64.7%)	6 (66.7%)	5 (62.5%)
<b>Current smoker</b>	0 (0.0%)	0 (0.0%)	0 (0.0%)
<b>ESKD cause</b> DN HTN/vascular GN/autoimmune Genetic Other/unknown	10 (58.8%) 0 (0.0%) 1 (5.9%) 0 (0.0%) 6 (35.3%)	6 (66.7%) 0 (0.0%) 0 (0.0%) 0 (0.0%) 3 (33.3%)	4 (50.0%) 0 (0.0%) 1 (12.5%) 0 (0.0%) 3 (37.5%)
<b>Hospitalisation due to COVID-19†</b>	9 (52.9%)	1 (11.1%)	8 (100%)
<b>Fatal COVID-19</b>	4 (23.5%)	0 (0.0%)	4 (50.0%)

DN = diabetic nephropathy. GN = glomerulonephritis. HTN = hypertension. IQR = inter-quartile range. Subsets defined according to peak WHO severity over the course of the illness.

**Supplementary Table 3: Transcriptomic modules associated with disease trajectory.**

Module code	Module name	Size	Selected enrichments	Primary cell type	Hub genes	Severity association
<b>tB</b>	Granulocyte cell-like module 1	1,309	R: Neutrophil degranulation R: Innate immune system R: ROS and RNS production in phagocytes R: Oxidative stress-induced senescence	Neutrophils	<i>TECPR2, CSF3R, STX3, MMP25, BASP1, MBOAT7, NCF4, GLT1D1, RNF24, DHX34</i>	↑
<b>tJ</b>	Granulocyte cell-like module 2	169	R: Neutrophil degranulation R: Innate immune system R: Antimicrobial peptides NABA: Matrisome	Macrophages (M0)	<i>CEACAM8, BPI, CD24, CEACAM6, ABCA13, DEFA4, LTF, AZU1, ELANE, LCN2</i>	↑*
<b>tL</b>	Plasma cell module	655	R: Cell cycle R: MHC class II antigen presentation WP: DNA damage response R: Factors involved in megakaryocyte development and platelet production	Plasma cells	<i>RRM2, FOXM1, MKI67, TPX2, BUB1, KIFC1, TK1, MZB1, CDK1, CCNA2</i>	↑
<b>tP</b>	Nuclear and cell cycle module	464	None significant	B cells naive	<i>SNRPA1, CEP95, THUMPD2, CENPC, ZNF326, NDUFAF5, ILKAP, SUPV3L1, USP36, GOLT1B</i>	↓
<b>tC</b>	T-cell activity module 1	545	KEGG: Natural killer cell mediated cytotoxicity R: Immunoregulatory interactions between a lymphoid and a non-lymphoid cell PID: CD8 TCR downstream pathway	NK cells resting	<i>SAMD3, ADGRG1, ZAP70, PYHIN1, FCRL6, PRSS23, FGFBP2, NFATC2, PTCH1, LLGL2</i>	↓
<b>tF</b>	T-cell activity module 2	761	WP: T-cell receptor and co-stimulatory signaling	T cells CD4 memory resting	<i>PLCG1, LCK, UBASH3A, ABCD2, LINC00649, PRKCQ-AS1, TC2N, LINC01550, SEPTIN1, NLRC3</i>	↓
<b>tI</b>	Monocyte module	299	R: PD1 signaling KEGG: Viral myocarditis KEGG: Antigen processing and presentation KEGG: Cell adhesion molecules R: Interferon gamma signaling	Monocytes	<i>PLXNB2, NAAA, CSF1R, PSAP, CARD9, SLC7A7, PEA15, ARHGEF10L, ZNF385A, ARRB1</i>	↓
<b>tN</b>	Allergy-related module	54	WP: IL-3 signaling pathway KEGG: Asthma	T cells CD4 memory resting	<i>HDC, LINC02458, CPA3, GATA2, AKAP12, MS4A2, ENPP3, FCER1A, TRIM51EP, SLC45A3</i>	↓

Transcriptomic modules associated with disease trajectory (i.e. with a significant TxCC interaction) are tabulated and assigned names that are representative of their members. Size = the number of genes assigned to the module. Primary cell type indicates the CIBERSORTx cell type with the greatest positive correlation with the module's eigengene. Severity association indicates whether the module's eigengene is positively (↑) or negatively (↓) associated with contemporaneous WHO severity (5% FDR).

\* Module tJ was positively correlated with severity, but this association was not significant at 5% FDR.

R = Reactome

WP = WikiPathways

PID = Pathway Interaction Database

**Supplementary Table 4: Proteomic modules associated with disease trajectory.**

Module code	Module name	Size	Selected enrichments	Hub genes	Severity association
p12	Histone-associated module	40	R: HDACs deacetylate histones KEGG: Systemic lupus erythematosus R: Chromatin modifying enzymes R: HCMV late events	H2AC1, H2AW, H2BU1, H2BC21, H2BC12, H2AZ1, CELF2, H2AC11, EEF1B2, MMP17	↑
p9	Splicing and nuclear module 1	241	PID: FRA pathway WP: Striated muscle contraction R: Complement cascade KEGG: Spliceosome	CLSTN3, KHSRP, OIT3, NELFA, EWSR1, CETP, PUF60, SRSF6, NXT1, ARHGAP36	↑
p8	Splicing and nuclear module 2	107	R: Processing of capped intron containing pre-mRNA R: mRNA splicing KEGG: Spliceosome	CILP, FUBP1, TSSC4, ALKAL2, STMN3, STMN1, STMN2, UBE2Z, MAFG, LEMD1	↑
p1	Mixed immune module 1	281	WP: Development of pulmonary dendritic cells and macrophage subsets	MRPL52, PLA2G2C, ITGAL, NLRP4, GDF3, VSTM4, ITGB1, SVBP, ANXA8, UBD	↑
p7	Mixed immune module 2	66	None significant	DEFB135, SPINK14, VAT1L, NT5E, PAXIP1, ZHX3, ODC1, PLEKHM2, DEFB112, F3	↓

Proteomic modules associated with disease trajectory (i.e. with a significant TxCC interaction) are tabulated and assigned names that are representative of their members. Size = the number of proteins assigned to the module. Severity association indicates whether the module's eigenprotein is positively ( ↑ ) or negatively ( ↓ ) associated with contemporaneous WHO severity (5% FDR).

R = Reactome

WP = WikiPathways

PID = Pathway Interaction Database

1349 **Supplementary Table 5. List of antibodies used in flow cytometry.**

Antibodies	Source	Clone	Identifier
BV421-CD4	BioLegend	A161A1	357424
BV421-CD14	BioLegend	63D3	367144
PB-CD57	BioLegend	QA17A04	393316
PB-Foxp3 (Intracellular)	BioLegend	206D	320116
BV510-CD95	BioLegend	DX2	305640
BV510-IgD	BioLegend	IA6-2	348219
BV605-CCR7	BioLegend	G043H7	353224
BV605-CD4	BioLegend	SK3	344645
BV650-HLA-DR	BioLegend	L243	307650
BV650-CD123	BioLegend	6H6	306032
BV711-KLRG1	BioLegend	2F1/KLRG1	138427
BV711-CD11c	BioLegend	3.9	301630
BV750-CD45RA	BioLegend	HI100	304166
BV750-HLA-DR	BioLegend	L243	307672
BV785-CD19	BioLegend	HIB19	302240
AF488-CD3	BioLegend	HIT3a	300320
BB515-CD152/CTLA-4 (Intracellular)	BD Bioscience	BNI3	566917
BB515-CD8	BD Bioscience	RPA-T8	564526
PE-CD56	BioLegend	39D5	355504
PE-CD335	BioLegend	9 <sup>E</sup> 2	331908
PE- CD16	BioLegend	3G8	302008
PE- CD14	BioLegend	63D3	367104
PE- CD19	BioLegend	HIB19	302208
PE-Siglec-1	BioLegend	7-239	346004
PEDAZ594-CD69	BioLegend	FN50	310941
PEDAZ594-NKG2D	BioLegend	1D11	320828
PE-Cy5-CD27	Thermofisher	O323	15-0279-42
PE-Cy5-CD25	Biolegend	BC96	302608
Percp-cy5.5-Ki67 (Intracellular)	BioLegend	Ki-67	350520
Percp-ef710-gdTCR	Thermofisher	B1.1	46-9959-42
Percp-ef710-CD16	Thermofisher	CB16	46-0168-42
PE-Cy7-PD1	BioLegend	A17188B	621616
PE-Cy7-CD141	Biolegend	M80	344110
AF647-CD45	BioLegend	HI30	304056
AF700-CD8	BioLegend	HIT8a	300920
AF700-CD66b	BioLegend	VI MA81	305114
APC/Fire750-CD38	BioLegend	HB-7	356626

1350

1351

1352 **Titles for Supplementary File - (in Excel file)**

1353 **Supplementary File 1A. Differential gene expression analysis comparing COVID-19**  
1354 **positive versus negative PBMC samples.** Contains the linear mixed model estimates and  
1355 corresponding P-values for each gene, for both the Wave 1 and Wave 2 cohorts. The column  
1356 “Aggregated Score” represents the RRA score for the P-values from both cohorts.

1357 **Supplementary File 1B. Gene set analysis comparing COVID-19 positive versus**  
1358 **negative samples.** Contains the linear mixed model estimates and corresponding P-values  
1359 for each GSVA gene set, for both the Wave 1 and Wave 2 cohorts. The column “Aggregated  
1360 Score” represents the RRA score for the P-values from both cohorts.

1361 **Supplementary File 1C. Protein annotations.** List of proteins measured by the SomaScan  
1362 v4.1 assay, their corresponding UniProt and GeneIDs, and their annotations in the human  
1363 protein atlas.

1364 **Supplementary File 1D. Differential plasma protein abundance analysis comparing**  
1365 **COVID-19 positive versus negative samples.** Contains the linear mixed model estimates  
1366 and corresponding P-values for each protein, for both the Wave 1 and Wave 2 cohorts. The  
1367 column “Aggregated Score” represents the RRA score for the P-values from both cohorts.

1368 **Supplementary File 1E. Protein set analysis comparing COVID-19 positive versus**  
1369 **negative samples.** Contains the linear mixed model estimates and corresponding P-values  
1370 for each GSVA protein set, for both the Wave 1 and Wave 2 cohorts. The column “Aggregated  
1371 Score” represents the RRA score for the P-values from both cohorts.

1372 **Supplementary File 1F. Transcriptomic associations with contemporaneous COVID-19**  
1373 **severity.** Associations with 4-level ordinal WHO severity score at the time of the sample.  
1374 Contains the linear mixed model estimates and corresponding P-values for each gene, for  
1375 both the Wave 1 and Wave 2 cohorts. The column “Aggregated Score” represents the RRA  
1376 score for the P-values from both cohorts.

1377 **Supplementary File 1G. Associations of gene sets with contemporaneous COVID-19**  
1378 **severity.** Associations with 4-level ordinal WHO severity score at the time of the sample.  
1379 Contains the linear mixed model estimates and corresponding P-values for each GSVA gene  
1380 set, for both the Wave 1 and Wave 2 cohorts. The column “Aggregated Score” represents the  
1381 RRA score for the P-values from both cohorts.

1382 **Supplementary File 1H. Proteomic associations with contemporaneous COVID-19**  
1383 **severity.** Associations with 4-level ordinal WHO severity score at the time of the sample.  
1384 Contains the linear mixed model estimates and corresponding P-values for each protein, for  
1385 both the Wave 1 and Wave 2 cohorts. The column “Aggregated Score” represents the RRA  
1386 score for the P-values from both cohorts.

1387 **Supplementary File 1I. Associations of protein sets with contemporaneous COVID-19**  
1388 **severity.** Associations with 4-level ordinal WHO severity score at the time of the sample.  
1389 Contains the linear mixed model estimates and corresponding P-values for each GSVA gene  
1390 set, for both the Wave 1 and Wave 2 cohorts. The column “Aggregated Score” represents the  
1391 RRA score for the P-values from both cohorts.

1392 **Supplementary File 1J. The membership of genes to WGCNA transcriptomic modules.**

1393 **Supplementary File 1K. The membership of proteins to WGCNA proteomic modules.**

- 1394 **Supplementary File 1L. Gene set enrichment of transcriptomic WGCNA modules.**  
1395 Overrepresentation analysis of gene sets for each module.
- 1396 **Supplementary File 1M. Protein set enrichment of proteomic WGCNA modules.**  
1397 Overrepresentation analysis of protein sets for each module.
- 1398 **Supplementary File 1N. Associations of imputed cell proportions with transcriptomic**  
1399 **WGCNA modules.** Contains the linear mixed model estimates and corresponding P-values  
1400 for each WGCNA module – imputed cell type pair.
- 1401 **Supplementary File 1O. Longitudinal profiles of cytokine proteins in plasma.** P-values  
1402 for the linear mixed modelling of cytokines and related proteins. P-values are included for the  
1403 time, clinical course, and time \* clinical course (TxCC) terms.
- 1404 **Supplementary File 1P. Importance metrics for supervised learning of the**  
1405 **transcriptome.** The relative importance of genes according to the random forests (accuracy  
1406 decrease) and lasso (number of models in which each gene had a non-zero coefficient during  
1407 cross-validation) models. The metrics are normalised such that the most important gene has  
1408 a value of 1.
- 1409 **Supplementary File 1Q. Importance metrics for supervised learning of the proteome.**  
1410 The relative importance of proteins according to the random forests (accuracy decrease) and  
1411 lasso (number of models in which each protein had a non-zero coefficient during cross-  
1412 validation) models. The metrics are normalised such that the most important gene has a value  
1413 of 1.
- 1414 **Supplementary File 1R. Multi-omic supervised learning importance metrics.** The relative  
1415 importance of features (genes or proteins) according to the random forests (accuracy  
1416 decrease) and lasso (number of models in which each feature had a non-zero coefficient  
1417 during cross-validation) models. The metrics are normalised such that the most important  
1418 gene has a value of 1.
- 1419 **Supplementary File 1S. Paired differential expression analysis of pre-infection versus**  
1420 **convalescent samples.** Contains the linear mixed model estimates and corresponding P-  
1421 values for each gene.
- 1422 **Supplementary File 1T. Gene set enrichment of convalescence analysis.** Contains the  
1423 linear mixed model estimates and corresponding P-values for each GSVA gene set, for both  
1424 the Wave 1 and Wave 2 cohorts. The column “Aggregated Score” represents the RRA score  
1425 for the P-values from both cohorts.
- 1426

## REFERENCES

1. Mann, E. R. *et al.* Longitudinal immune profiling reveals key myeloid signatures associated with COVID-19. *Sci. Immunol.* **5**, eabd6197 (2020) doi:10.1126/sciimmunol.abd6197.
2. Laing, A. G. *et al.* A dynamic COVID-19 immune signature includes associations with poor prognosis. *Nat. Med.* (2020) doi:10.1038/s41591-020-1038-6.
3. Stephenson, E. *et al.* Single-cell multi-omics analysis of the immune response in COVID-19. *Nat. Med.* **27**, 904–916 (2021) doi:10.1038/s41591-021-01329-2.
4. Bernardes, J. P. *et al.* Longitudinal Multi-omics Analyses Identify Responses of Megakaryocytes, Erythroid Cells, and Plasmablasts as Hallmarks of Severe COVID-19. *Immunity* **53**, 1296–1314.e9 (2020) doi:https://doi.org/10.1016/j.immuni.2020.11.017.
5. Szabo, P. A. *et al.* Longitudinal profiling of respiratory and systemic immune responses reveals myeloid cell-driven lung inflammation in severe COVID-19. *Immunity* **54**, 797–814.e6 (2021) doi:https://doi.org/10.1016/j.immuni.2021.03.005.
6. Bergamaschi, L. *et al.* Longitudinal analysis reveals that delayed bystander CD8+ T cell activation and early immune pathology distinguish severe COVID-19 from mild disease. *Immunity* **54**, 1257–1275.e8 (2021) doi:https://doi.org/10.1016/j.immuni.2021.05.010.
7. Ahern, D. J. *et al.* A blood atlas of COVID-19 defines hallmarks of disease severity and specificity. *Cell* **185**, 916–938.e58 (2022) doi:10.1016/j.cell.2022.01.012.
8. Filbin, M. R. *et al.* Longitudinal proteomic analysis of severe COVID-19 reveals survival-associated signatures, tissue-specific cell death, and cell-cell interactions. *Cell Reports Med.* **2**, 100287 (2021) doi:10.1016/j.xcrm.2021.100287.
9. Gisby, J. *et al.* Longitudinal proteomic profiling of dialysis patients with COVID-19 reveals markers of severity and predictors of death. *Elife* **10**, 2020.11.05.20223289 (2021) doi:10.7554/eLife.64827.
10. Rodriguez, L. *et al.* Systems-Level Immunomonitoring from Acute to Recovery Phase of Severe COVID-19. *Cell reports. Med.* **1**, 100078 (2020) doi:10.1016/j.xcrm.2020.100078.
11. Demichev, V. *et al.* A time-resolved proteomic and prognostic map of COVID-19. *Cell Syst.* **12**, 780–794.e7 (2021) doi:https://doi.org/10.1016/j.cels.2021.05.005.
12. Gutmann, C. *et al.* SARS-CoV-2 RNAemia and proteomic trajectories inform prognostication in COVID-19 patients admitted to intensive care. *Nat. Commun.* **12**, 3406 (2021) doi:10.1038/s41467-021-23494-1.
13. Galbraith, M. D. *et al.* Seroconversion stages COVID19 into distinct pathophysiological states. *Elife* **10**, e65508 (2021) doi:10.7554/eLife.65508.
14. Paranjpe, I. *et al.* Proteomic Characterization of Acute Kidney Injury in Patients Hospitalized with SARS-CoV2 Infection. *medRxiv* 2021.12.09.21267548 (2021) doi:10.1101/2021.12.09.21267548.
15. Su, C.-Y. *et al.* Circulating proteins to predict adverse COVID-19 outcomes. *medRxiv* 2021.10.04.21264015 (2021) doi:10.1101/2021.10.04.21264015.
16. Sullivan, K. D. *et al.* The COVIDome Explorer researcher portal. *Cell Rep.* **36**, (2021) doi:10.1016/j.celrep.2021.109527.
17. Horby, P. *et al.* Dexamethasone in Hospitalized Patients with Covid-19. *N. Engl. J. Med.* **384**, 693–704 (2021) doi:10.1056/NEJMoa2021436.

- 1471 18. Gordon, A. C. *et al.* Interleukin-6 Receptor Antagonists in Critically Ill Patients with  
1472 Covid-19. *N. Engl. J. Med.* **384**, 1491–1502 (2021) doi:10.1056/NEJMoa2100433.
- 1473 19. Tocilizumab in patients admitted to hospital with COVID-19 (RECOVERY): a  
1474 randomised, controlled, open-label, platform trial. *Lancet (London, England)* **397**,  
1475 1637–1645 (2021) doi:10.1016/S0140-6736(21)00676-0.
- 1476 20. Kalil, A. C. *et al.* Baricitinib plus Remdesivir for Hospitalized Adults with Covid-19. *N.*  
1477 *Engl. J. Med.* **384**, 795–807 (2021) doi:10.1056/NEJMoa2031994.
- 1478 21. Williamson, E. J. *et al.* Factors associated with COVID-19-related death using  
1479 OpenSAFELY. *Nature* **584**, 430–436 (2020) doi:10.1038/s41586-020-2521-4.
- 1480 22. Goffin, E. *et al.* COVID-19-related mortality in kidney transplant and haemodialysis  
1481 patients: a comparative, prospective registry-based study. *Nephrol. Dial. Transplant.*  
1482 *Off. Publ. Eur. Dial. Transpl. Assoc. - Eur. Ren. Assoc.* **36**, 2094–2105 (2021)  
1483 doi:10.1093/ndt/gfab200.
- 1484 23. Chen, J.-J. *et al.* Immunogenicity Rates After SARS-CoV-2 Vaccination in People With  
1485 End-stage Kidney Disease: A Systematic Review and Meta-analysis. *JAMA Netw.*  
1486 *open* **4**, e2131749 (2021) doi:10.1001/jamanetworkopen.2021.31749.
- 1487 24. Anand, S. *et al.* Antibody Response to COVID-19 Vaccination in Patients Receiving  
1488 Dialysis. *J. Am. Soc. Nephrol.* **32**, 2435–2438 (2021) doi:10.1681/ASN.2021050611.
- 1489 25. Hänzelmann, S., Castelo, R. & Guinney, J. GSVA: gene set variation analysis for  
1490 microarray and RNA-Seq data. *BMC Bioinformatics* **14**, 7 (2013) doi:10.1186/1471-  
1491 2105-14-7.
- 1492 26. Wilk, A. J. *et al.* A single-cell atlas of the peripheral immune response in patients with  
1493 severe COVID-19. *Nat. Med.* **26**, 1070–1076 (2020) doi:10.1038/s41591-020-0944-y.
- 1494 27. Liu, G. *et al.* ISG15-dependent activation of the sensor MDA5 is antagonized by the  
1495 SARS-CoV-2 papain-like protease to evade host innate immunity. *Nat. Microbiol.* **6**,  
1496 467–478 (2021) doi:10.1038/s41564-021-00884-1.
- 1497 28. Hachim, M. Y. *et al.* Interferon-Induced Transmembrane Protein (IFITM3) Is  
1498 Upregulated Explicitly in SARS-CoV-2 Infected Lung Epithelial Cells. *Front. Immunol.*  
1499 **11**, 1372 (2020) doi:10.3389/fimmu.2020.01372.
- 1500 29. Langfelder, P. & Horvath, S. WGCNA: An R package for weighted correlation network  
1501 analysis. *BMC Bioinformatics* **9**, (2008) doi:10.1186/1471-2105-9-559.
- 1502 30. Velten, B., Braunger, J. M., Arnol, D., Argelaguet, R. & Stegle, O. Identifying temporal  
1503 and spatial patterns of variation from multi-modal data using MEFISTO. *bioRxiv*  
1504 2020.11.03.366674 (2020) doi:10.1101/2020.11.03.366674.
- 1505 31. Bagheri-Hosseiniabadi, Z., Abbasi, M., Kahnouji, M., Ghorbani, Z. & Abbasifard, M. The  
1506 prognostic value of S100A calcium binding protein family members in predicting severe  
1507 forms of COVID-19. *Inflamm. Res.* **71**, 369–376 (2022) doi:10.1007/s00011-022-  
1508 01545-7.
- 1509 32. Schett, G., McInnes, I. B. & Neurath, M. F. Reframing Immune-Mediated Inflammatory  
1510 Diseases through Signature Cytokine Hubs. *N. Engl. J. Med.* **385**, 628–639 (2021)  
1511 doi:10.1056/NEJMra1909094.
- 1512 33. Shilts, J. *et al.* LRRC15 mediates an accessory interaction with the SARS-CoV-2 spike  
1513 protein. *bioRxiv* 2021.09.25.461776 (2021) doi:10.1101/2021.09.25.461776.
- 1514 34. Song, J. *et al.* LRRC15 is an inhibitory receptor blocking SARS-CoV-2 spike-mediated  
1515 entry in trans. *bioRxiv: the preprint server for biology* (2021)

- doi:10.1101/2021.11.23.469714.
35. Ng, J. H. *et al.* Outcomes of patients with end-stage kidney disease hospitalized with COVID-19. *Kidney Int.* (2020) doi:10.1016/j.kint.2020.07.030.
36. Mei, Q. *et al.* Regulation of DNA replication-coupled histone gene expression. *Oncotarget* **8**, 95005–95022 (2017) doi:10.18632/oncotarget.21887.
37. Singh, R. K., Kabbaj, M.-H. M., Paik, J. & Gunjan, A. Histone levels are regulated by phosphorylation and ubiquitylation-dependent proteolysis. *Nat. Cell Biol.* **11**, 925–933 (2009) doi:10.1038/ncb1903.
38. Silk, E., Zhao, H., Weng, H. & Ma, D. The role of extracellular histone in organ injury. *Cell Death Dis.* **8**, e2812 (2017) doi:10.1038/cddis.2017.52.
39. Bojkova, D. *et al.* Proteomics of SARS-CoV-2-infected host cells reveals therapy targets. *Nature* **583**, 469–472 (2020) doi:10.1038/s41586-020-2332-7.
40. Finkel, Y. *et al.* SARS-CoV-2 uses a multipronged strategy to impede host protein synthesis. *Nature* **594**, 240–245 (2021) doi:10.1038/s41586-021-03610-3.
41. Vlahos, R. *et al.* Inhibition of Nox2 Oxidase Activity Ameliorates Influenza A Virus-Induced Lung Inflammation. *PLOS Pathog.* **7**, e1001271 (2011).
42. Lang, P. A. *et al.* Reactive oxygen species delay control of lymphocytic choriomeningitis virus. *Cell Death Differ.* **20**, 649–658 (2013) doi:10.1038/cdd.2012.167.
43. Randzavola, L. O. *et al.* EROS-mediated control of NOX2 and P2X7 biosynthesis. *bioRxiv* 2021.09.14.460103 (2021) doi:10.1101/2021.09.14.460103.
44. Ng, B., Cook, S. A. & Schafer, S. Interleukin-11 signaling underlies fibrosis, parenchymal dysfunction, and chronic inflammation of the airway. *Exp. Mol. Med.* **52**, 1871–1878 (2020) doi:10.1038/s12276-020-00531-5.
45. Schafer, S. *et al.* IL-11 is a crucial determinant of cardiovascular fibrosis. *Nature* **552**, 110–115 (2017) doi:10.1038/nature24676.
46. Kiernan, K. & MacIver, N. J. The Role of the Adipokine Leptin in Immune Cell Function in Health and Disease. *Front. Immunol.* **11**, 622468 (2020) doi:10.3389/fimmu.2020.622468.
47. Segerer, S. E. *et al.* The glycoprotein-hormones activin A and inhibin A interfere with dendritic cell maturation. *Reprod. Biol. Endocrinol.* **6**, 17 (2008) doi:10.1186/1477-7827-6-17.
48. Rapp, M. *et al.* CCL22 controls immunity by promoting regulatory T cell communication with dendritic cells in lymph nodes. *J. Exp. Med.* **216**, 1170–1181 (2019) doi:10.1084/jem.20170277.
49. Zhang, Q. *et al.* Inborn errors of type I IFN immunity in patients with life-threatening COVID-19. *Science* **370**, (2020) doi:10.1126/science.abd4570.
50. Bastard, P. *et al.* Autoantibodies against type I IFNs in patients with life-threatening COVID-19. *Science* **370**, (2020) doi:10.1126/science.abd4585.
51. Ho, F. K. *et al.* Thromboembolic Risk in Hospitalized and Nonhospitalized COVID-19 Patients: A Self-Controlled Case Series Analysis of a Nationwide Cohort. *Mayo Clin. Proc.* **96**, 2587–2597 (2021) doi:10.1016/j.mayocp.2021.07.002.
52. Gorog, D. A. *et al.* Current and novel biomarkers of thrombotic risk in COVID-19: a Consensus Statement from the International COVID-19 Thrombosis Biomarkers

- 1559 Colloquium. *Nat. Rev. Cardiol.* 1–21 (2022) doi:10.1038/s41569-021-00665-7.
- 1560 53. Katsoularis, I. *et al.* Risks of deep vein thrombosis, pulmonary embolism, and bleeding  
1561 after covid-19: nationwide self-controlled cases series and matched cohort study. *BMJ*  
1562 **377**, (2022) doi:10.1136/bmj-2021-069590.
- 1563 54. Greinacher, A. *et al.* Thrombotic Thrombocytopenia after ChAdOx1 nCov-19  
1564 Vaccination. *N. Engl. J. Med.* **384**, 2092–2101 (2021) doi:10.1056/NEJMoa2104840.
- 1565 55. Schultz, N. H. *et al.* Thrombosis and Thrombocytopenia after ChAdOx1 nCoV-19  
1566 Vaccination. *N. Engl. J. Med.* **384**, 2124–2130 (2021) doi:10.1056/NEJMoa2104882.
- 1567 56. Greinacher, A. *et al.* Insights in ChAdOx1 nCoV-19 vaccine-induced immune thrombotic  
1568 thrombocytopenia. *Blood* **138**, 2256–2268 (2021) doi:10.1182/blood.2021013231.
- 1569 57. Ewels, P. A. *et al.* The nf-core framework for community-curated bioinformatics  
1570 pipelines. *Nat. Biotechnol.* **38**, 276–278 (2020) doi:10.1038/s41587-020-0439-x.
- 1571 58. Di Tommaso, P. *et al.* Nextflow enables reproducible computational workflows. *Nat.*  
1572 *Biotechnol.* **35**, 316–319 (2017) doi:10.1038/nbt.3820.
- 1573 59. Andrews, S. *et al.* FastQC: a quality control tool for high throughput sequence data.  
1574 (2012).
- 1575 60. Martin, M. Cutadapt removes adapter sequences from high-throughput sequencing  
1576 reads. *EMBnet.journal; Vol 17, No 1 Next Gener. Seq. Data Anal.* -  
1577 *10.14806/ej.17.1.200* (2011).
- 1578 61. Dobin, A. *et al.* STAR: ultrafast universal RNA-seq aligner. *Bioinformatics* **29**, 15–21  
1579 (2013) doi:10.1093/bioinformatics/bts635.
- 1580 62. Anders, S., Pyl, P. T. & Huber, W. HTSeq--a Python framework to work with high-  
1581 throughput sequencing data. *Bioinformatics* **31**, 166–169 (2015)  
1582 doi:10.1093/bioinformatics/btu638.
- 1583 63. Robinson, M. D., McCarthy, D. J. & Smyth, G. K. edgeR: a Bioconductor package for  
1584 differential expression analysis of digital gene expression data. *Bioinformatics* **26**, 139–  
1585 140 (2010) doi:10.1093/bioinformatics/btp616.
- 1586 64. Robinson, M. D. & Oshlack, A. A scaling normalization method for differential  
1587 expression analysis of RNA-seq data. *Genome Biol.* **11**, R25 (2010) doi:10.1186/gb-  
1588 2010-11-3-r25.
- 1589 65. Howe, K. L. *et al.* Ensembl 2021. *Nucleic Acids Res.* **49**, D884–D891 (2021)  
1590 doi:10.1093/nar/gkaa942.
- 1591 66. Tweedie, S. *et al.* Genenames.org: the HGNC and VGNC resources in 2021. *Nucleic*  
1592 *Acids Res.* **49**, D939–D946 (2021) doi:10.1093/nar/gkaa980.
- 1593 67. John, C. R. *et al.* M3C: Monte Carlo reference-based consensus clustering. *Sci. Rep.*  
1594 **10**, 1–14 (2020) doi:10.1038/s41598-020-58766-1.
- 1595 68. Uhlen, M. *et al.* Tissue-based map of the human proteome. *Science (80-. ).* **347**,  
1596 1260419–1260419 (2015) doi:10.1126/science.1260419.
- 1597 69. Bates, D., Mächler, M., Bolker, B. & Walker, S. Fitting Linear Mixed-Effects Models  
1598 Using lme4. *J. Stat. Softw.* **67**, (2015) doi:10.18637/jss.v067.i01.
- 1599 70. Kuznetsova, A., Brockhoff, P. B. & Christensen, R. H. B. lmerTest Package: Tests in  
1600 Linear Mixed Effects Models. *J. Stat. Softw.* **82**, (2017) doi:10.18637/jss.v082.i13.
- 1601 71. Hoffman, G. E. & Roussos, P. Dream: powerful differential expression analysis for

1602 repeated measures designs. *Bioinformatics* **37**, 192–201 (2021)  
1603 doi:10.1093/bioinformatics/btaa687.

1604 72. Hoffman, G. E. & Schadt, E. E. variancePartition: interpreting drivers of variation in  
1605 complex gene expression studies. *BMC Bioinformatics* **17**, 483 (2016)  
1606 doi:10.1186/s12859-016-1323-z.

1607 73. Liberzon, A. *et al.* Molecular signatures database (MSigDB) 3.0. *Bioinformatics* **27**,  
1608 1739–1740 (2011) doi:10.1093/bioinformatics/btr260.

1609 74. Buang, N. *et al.* Type I interferons affect the metabolic fitness of CD8+ T cells from  
1610 patients with systemic lupus erythematosus. *Nat. Commun.* **12**, 1980 (2021)  
1611 doi:10.1038/s41467-021-22312-y.

1612 75. Kolde, R., Laur, S., Adler, P. & Vilo, J. Robust rank aggregation for gene list integration  
1613 and meta-analysis. *Bioinformatics* **28**, 573–580 (2012)  
1614 doi:10.1093/bioinformatics/btr709.

1615 76. Li, J. *et al.* Application of Weighted Gene Co-expression Network Analysis for Data from  
1616 Paired Design. *Sci. Rep.* **8**, 622 (2018) doi:10.1038/s41598-017-18705-z.

1617 77. Bakdash, J. Z. & Marusich, L. R. Repeated measures correlation. *Front. Psychol.* **8**, 1–  
1618 13 (2017) doi:10.3389/fpsyg.2017.00456.

1619 78. Langfelder, P., Zhang, B. & Horvath, S. Defining clusters from a hierarchical cluster  
1620 tree: The Dynamic Tree Cut package for R. *Bioinformatics* **24**, 719–720 (2008)  
1621 doi:10.1093/bioinformatics/btm563.

1622 79. Perperoglou, A., Sauerbrei, W., Abrahamowicz, M. & Schmid, M. A review of spline  
1623 function procedures in R. *BMC Med. Res. Methodol.* **19**, 1–16 (2019)  
1624 doi:10.1186/s12874-019-0666-3.

1625 80. Wu, T. *et al.* clusterProfiler 4.0: A universal enrichment tool for interpreting omics data.  
1626 *Innov.* **2**, 100141 (2021) doi:https://doi.org/10.1016/j.xinn.2021.100141.

1627 81. Newman, A. M. *et al.* Determining cell type abundance and expression from bulk tissues  
1628 with digital cytometry. *Nat. Biotechnol.* **37**, 773–782 (2019) doi:10.1038/s41587-019-  
1629 0114-2.

1630 82. Newman, A. M. *et al.* Robust enumeration of cell subsets from tissue expression  
1631 profiles. *Nat. Methods* **12**, 453–457 (2015) doi:10.1038/nmeth.3337.

1632 83. Velten, B. *et al.* Identifying temporal and spatial patterns of variation from multimodal  
1633 data using MEFISTO. *Nat. Methods* **19**, (2022) doi:10.1038/s41592-021-01343-9.

1634 84. Kuhn, M. Building Predictive Models in R Using the caret Package. *J. Stat. Softw.* **28**,  
1635 1–26 (2008) doi:10.18637/jss.v028.i05.

1636 85. Friedman, J. H., Hastie, T. & Tibshirani, R. Regularization Paths for Generalized Linear  
1637 Models via Coordinate Descent. *J. Stat. Softw.* **33**, 1–22 (2010)  
1638 doi:10.18637/jss.v033.i01.

1639